The Pennsylvania State University
The Graduate School

A STUDY ON THE ANALYSIS OF THE FORMATION OF HIGH WATER SATURATION ZONES AROUND WELL PERFORATIONS

A Dissertation in
Petroleum and Mineral Engineering
by
Muhammad Alrumah

Submitted in Partial Fulfillment
of the Requirements
for the Degree of

Doctor of Philosophy

December 2011

The dissertation of Muhammad Alrumah was reviewed and approved* by the following:

Turgay Ertekin
Professor of Petroleum and Natural Gas Engineering
Dissertation Advisor, Chair of Committee

Robert Watson
Associate Professor Emeritus of Petroleum and Natural Gas Engineering

John Yilin Wang
Assistant Professor of Petroleum and Natural Gas Engineering

Li Li
Associate Professor of Petroleum and Natural Gas Engineering

Savash Yavuzkurt
Professor of Mechanical Engineering

R. Larry Grayson
Graduate Program Officer of Energy and Mineral Engineering

*Signatures are on file in the Graduate School.

Abstract

The water produced with oil as a result of water coning is a serious problem as it decreases well productivity and increases the cost of operation. The main cause of water coning is the pressure drawdown near the wellbore. Producing a well in an oil reservoir with a bottom water drive will cause the original oil-water contact to rise towards the well in the shape of a cone. As production continues, the height of the cone increases. Once the water reaches the wellbore, the water starts to be produced and water production increases with time while the oil production decreases.

The first part of this thesis is concerned with the analysis of pressure transient data in an oil reservoir with edge water. A *3-D* numerical model is used to generate pressure transient data for a vertical well. The reservoir is considered as a composite reservoir where the inner zone contains the oil phase, and the outer zone contains the water phase. Procedures are proposed to help estimate the distance to the discontinuity under certain conditions. These procedures can be applied using the derivative of the pressure buildup test data if the mobility ratio is less than unity. Some of the parameters that control the accuracy of the proposed analysis procedure are the producing time and the external reservoir radius.

The second part of this study is concerned with the water coning phenomena. Artificial neural networks are developed to predict water saturation around vertical and horizontal wells with a good accuracy in oil reservoirs experiencing a bottom water drive. The data used to develop the neural networks are from a numerical simulation model for reservoirs created using synthetic data. The neural networks have been found to effectively predict the change of water saturation over the time and show the development of the water cone.

Table of Contents

List of Figures

List of Tables

List of Symbols

B	Formation volume factor, bbl/STB, p. 12
C1	Constant in the system of equations, p. 10
C2	Constant in the system of equations, p. 10
C3	Constant in the system of equations, p. 10
C	Wellbore storage coefficient, bbl/psi, p. 12
C_D	Dimensionless wellbore storage coefficient, p. 9
c_t	total compressibility, psi^{-1}, p. 11
F_s	Storativity ratio, p. 17
h	Total reservoir thickness, ft, p. 7
h_d	Depth of the horizontal well from the top of the pay zone, ft, p. **??**
h_L	Length of the horizontal well, ft, p. **??**
h_p	Length of the open-to-flow thickness of the pay zone, ft, p. 69
I	Modified Bessel Function of the first kind, p. 10
K	Modified Bessel Function of the second kind, p. 10
k	Absolute permeability, md, p. 11
k_r	Permeability in the r-direction in radial system, md, p. 36
k_v	Permeability in the veritical direction in radial system, md, p. 69

k_x Permeability in the x-direction in rectangular system, md, p. 36

k_y Permeability in the u-direction in rectangular system, md, p. 36

p_i Initial reservoir pressure, psi, p. 7

p_w Wellbore pressure, psi, p. 12

p_{ws} Wellbore shut-in pressure, psi, p. 35

q_L Total liquid flow rate, STB/D, p. 69

r_e Reservoir radius, ft, p. 7

r_{in} Distance to the discontinuity in the composite reservoir, ft, p. 2

r_{inv} Radius of investigation, ft, p. 19

$r_{(peak)}$ Radius of investigation calculated using $t_{(peak)}$, ft, p. 19

r_w Wellbore radius, ft, p. 11

S Skin factor, p. 9

s Laplace parameter, p. 10

S_{oi} Initial oil saturation, p. 36

S_w Water saturation, p. 41

t Time, hours, p. 12

t_{in} Time needed for the pressure transient to reach the discontinuity in a composite reservoir, hours, p. 24

t_p Producing time prior to shut-in, hours, p. 2

$t_{(peak)}$ Time at the peak in pressure derivative curve , hours, p. 19

α Parameter in the system of equation, p. 10

Δt Shut-in time, hours, p. 14

Δt_e Equivalent time, hours, p. 13

η Hydraulic diffusivity, p. 9

λ Mobility ratio, p. 11

μ Viscosity, cp, p. 11

ρ_o Oil Density, lb/ft^3, p. 81

ϕ Porosity, fraction, p. 7

Subscript

1 Inner zone of the composite reservoir, p. 9

2 Outer zone of the composite reservoir, p. 9

D Dimensionless parameter, p. 9

Acknowledgments

I would like to express my sincere gratitude and appreciation to my advisor and mentor Prof. Turgay Ertekin for his support, help, encouragement, patience and guidance during my work in my thesis. Also, I would like to extend my gratitude to my committee members Dr. Robert Watson, Dr. John Yilin Wang, Dr. Li Li, and Dr. Savash Yavuzkurt for their interest and for providing valuable suggestions and comments.

I would like to thank K. Patel from CMG for his technical support. Also I would like to thank my colleagues Mohammed Alabbad, Mohammad Alajmi, Talal Almousa, Yogesh Bansal, Eduardo Radespiel, and Emre Artun for their help, support, encouragement, and great friendship.

I would like to thank my parents, wife, and my brothers and sisters for their help, support, and patience.

Dedication

All Praise be to Allah, Cherisher and Sustainer of Worlds, who bestowed me with life and health to complete this work.

I wish to dedicate this work to my mother and my father for their continuous prayer and patience.

I dedicate this work to my wife for her sacrifices of her health, time, and professional progress to provide me with a comfortable environment. Her patience and encouragement was a drive for me to finish this work.

I dedicate this work to my children, Yousuf, Omar, and Dhuha. They fill my life with happiness and hope.

I dedicate this work to my brothers and sisters for their encouragement and prayers.

Chapter 1

Introduction

Many hydrocarbon reservoirs contain an active water aquifer. The drilled wells are always completed to produce hydrocarbon. As oil production continues, water starts to appear in the wellbore. This water is undesirable as its presence around the wellbore decreases the well productivity and needs more facilities to be handled, treated and disposed of at the surface resulting in extra investments and operating costs. Production of the hydrocarbon is initiated by the drawdown created at the wellbore, which causes a force that pulls the hydrocarbon towards the wellbore. This force also, with the capillary pressure, brings water in the aquifer upward towards the wellbore. What controls the height of the water is the gravitational force working in the opposite direction. The height of the water cone stops increasing if the upward dynamic flow forces become equal to the downward gravitational forces. The water will be produced once the height of the water reaches the wellbore. By continuing to produce the hydrocarbon with water, formation around the wellbore will be saturated with water in the shape of a cone, a phenomenon that is referred to as water coning.

This study consists of two parts. The first part studied the pressure transient test data for a vertical well in an oil reservoir with edge water (Fig 1.1). The reservoir was considered as a composite reservoir. A reservoir is composite when there is a difference in fluid properties or rock properties in two or more concentric zones in the reservoirs. In this part, the inner zone contains the oil phase, and the outer zone contains the water phase. This study will look into three cases of two-regions

composite reservoirs:

1. Two different absolute permeabilities
2. Two different hydrocarbon liquids (low viscosity oil and high viscosity oil)
3. Two different fluids (oil and water)

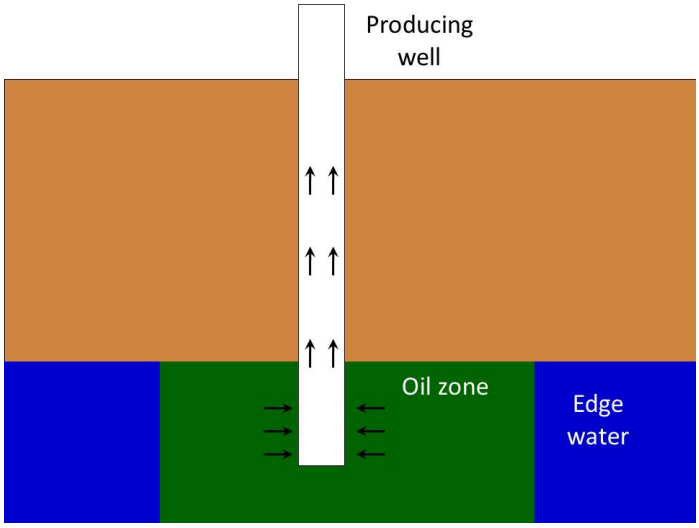

Figure 1.1: Schematic representation of an oil reservoir exposed to edge water encroachment.

The distance from the well to the interface that separates the two different zones in a composite reservoir is called the distance to the discontinuity (r_{in}), and it can be estimated from proposed procedures. The proposed procedures use the pressure derivative buildup data if the mobility ratio is less than unity. The main two factors that affect the accuracy of the estimate are the producing time (t_p) and the reservoir radius (r_e). These procedures can be used for an oil reservoir with edge water encroachment to monitor the distance to the edge water front over time to help in the future water handling plans.

The approach for this problem is done by going through 3 stages. The 1^{st} stage is analyzing the pressure transient data for an oil composite reservoir with two different absolute permeabilities. This simple case will assure that the value of r_{in} will not change during the life of the reservoir and limit the effects on the pressure

transient data with the effect of the discontinuity.
The 2^{nd} stage is more complex and involves analyzing a composite reservoir with two different oil viscosities. The value of r_{in} could change during the life of the reservoir as the produced oil in the inner zone will be displaced by the oil in the outer zone and this could change the value of r_{in}.
The 3^{rd} stage, which is the principal goal of this study, is analyzing a composite reservoir with two different fluids, oil and water. In this stage, the difference is not only for one property of a fluid, but instead, for two different fluids.

The second part analyzes the water coning phenomenon (Fig 1.2). The water coning behavior is very important in hydrocarbon production and the ability to predict its behavior will improve and help in better managing the reservoir. The behavior of the water coning in an oil reservoir was predicted successfully using artificial neural networks by predicting the change of the water saturation distribution in reservoirs over time. The developed neural networks were designed to be used for vertical and horizontal wells with a bottom water aquifer. These developed neural network can be useful in optimizing production to find the optimum perforation interval or the optimum production rate to delay the water production.

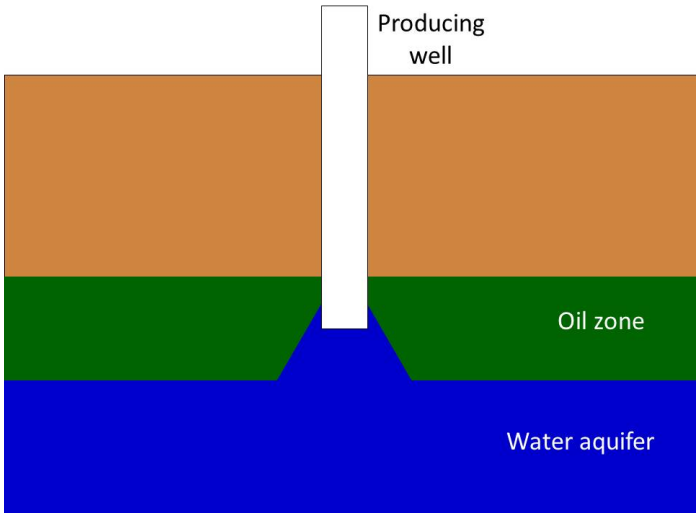

Figure 1.2: Schematic representation of an oil reservoir experiences water coning.

Chapter 2

Literature Review

2.1 Water Coning

The first paper which discussed the water coning phenomenon and its physics was *Muskat and Wyckoff (1935)*. In the paper it was indicated that some of the factors that affect the water coning are production rate and length of perforated interval. *Byrne and Morse (1973)*, *Mungan (1975)* and *Blades and Stright (1975)* performed a numerical study of the effects of various parameters on water coning in vertical wells. *Kuo and DesBrisay (1983)* also studied the effects of various parameters on water coning in vertical wells, and developed correlations to predict critical rate, breakthrough time and watercut after water production. *Yang and Wattenbarger (1991)* studied the water coning effects in vertical and horizontal wells and developed a method to calculate the critical rate, breakthrough time and the water-oil ratio after breakthrough. *Van Golf-Racht and Sonier (1994)* investigated the water coning behavior for a fractured reservoir in a vertical well and studied various parameters and their effects on the water coning.

Helle and Bhatt (2002) developed artificial neural networks that predict the underground fluids (water, oil and gas) from the well logs. *Shokir (2004)* presented new artificial neural networks that predict water saturation in shaly formation using the well log data and the core data as the inputs. *Al-Bulushi et al. (2009)* developed artificial neural networks models to predict water saturation from well log data and core data.

2.2 Composite Reservoirs

There have been many researchers interested in studying and analyzing composite reservoirs to understand their behavior and the flow performance under these conditions and also to calculate important parameters. *Hurst (1960)* and *Mortada (1960)* studied how the well performance is affected by the interference of two oil reservoirs producing from the same aquifer. *Carter (1966)* presented an analytical solution for a radial composite reservoir with a closed and no-flow outer boundary. He only changed the permeability in the two zones. *Satman et al. (1980)* presented another analytical solution for single phase systems with different fluid properties, two different permeabilities and an infinite reservoir. The wellbore storage and skin factors were taken into consideration. Regarding estimating the size and the distance to discontinuity in a composite reservoir, *Tang (1982)* showed that the intersection method can be used to determine the distance to the discontinuity if the pressure data include two well-defined semi-log straight lines. *Odeh (1969)* generated correlations to be used in trial and error to determine the mobility of the two zones in a radial composite reservoir and the distance to the discontinuity. *Bixel and Van Poollen (1967)* developed a method to calculate the distance to the discontinuity using type curves and then locating the deviation point to calculate the distance. *Loucks and Guerrero (1961)* found that under certain conditions, the permeabilities in both zones and the size of the inner zone can be determined from the pressure drawdown test. *Brown (1985)* presented graphical analysis to determine the mobility of the inner and the outer zones as well as the distance to the discontinuity. In using the semi-log plot to analyze pressure transient data, existing flow regimes need to be identified first. Also it is known that the pressure derivative response is more sensitive than the pressure data [*Bourdet et al. (1983)* and *Tiab and Kumar (1980)*]. *Issaka and Ambastha (1996)* developed a generalized pressure derivative formula for a composite reservoir to identify the flow regimes in four flow geometries (radial, elliptical, linear and spherical). *Olarewaju and Lee (1989)* found that the pressure derivative curves for a composite reservoir show a different response from homogenous reservoirs.

Chapter 3

Composite Reservoir Model

3.1 Numerical Model Development

Four 3D numerical models were used for the composite reservoir model study; two of the four models are single phase, oil models, and the other two are two-phase, oil/water models. All of the models are radial models with a vertical well. The radial grid system was used. The reservoir properties are homogeneous and isotropic and for the fluid properties, the reservoir conditions are assumed to be above bubblepoint pressure to ensure that no free gas is present in the reservoir. There is a base case for each model, and then, for each parameter to be studied, its value was changed to produce simulation runs for different values. The study domain used by the numerical model is shown in Fig 3.1 for the composite reservoir study. The model is populated by using homogeneous properties, isotropic permeability, single fluid in some cases and different fluids in other cases in each region. The reservoir is horizontal with uniform thickness. The model is verified against the analytical solution. The reservoir properties are tabulated in Table 3.1.

Table 3.1: Reservoir properties

thickness (h), ft	50
Porosity (ϕ)	0.25
Initial pressure (p_i), psig	5000
Temperature, ^{o}F	130
Reservoir radius (r_e), ft	6,000

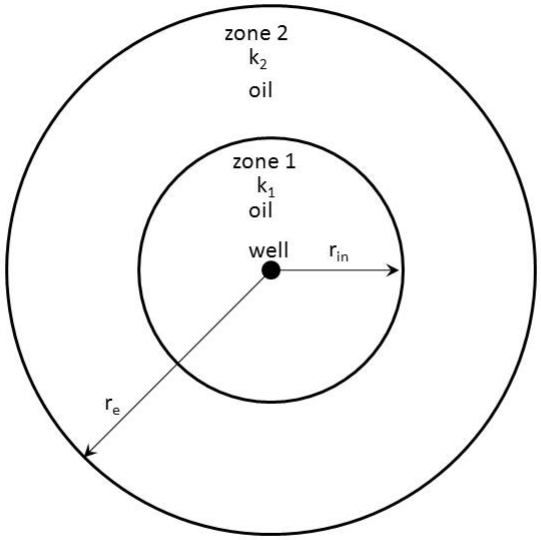

Figure 3.1: Schematic representation of a two-region radial composite reservoir

The absolute permeability in the vertical direction (z-direction) and the angular direction (θ-direction) are set equal to zero, so that the only component of the flow in the radial direction is analyzed. The gravitational forces are ignored. The model was run with two different scenarios (Fig 3.2) in order to gradually increase the complexity of the problem.

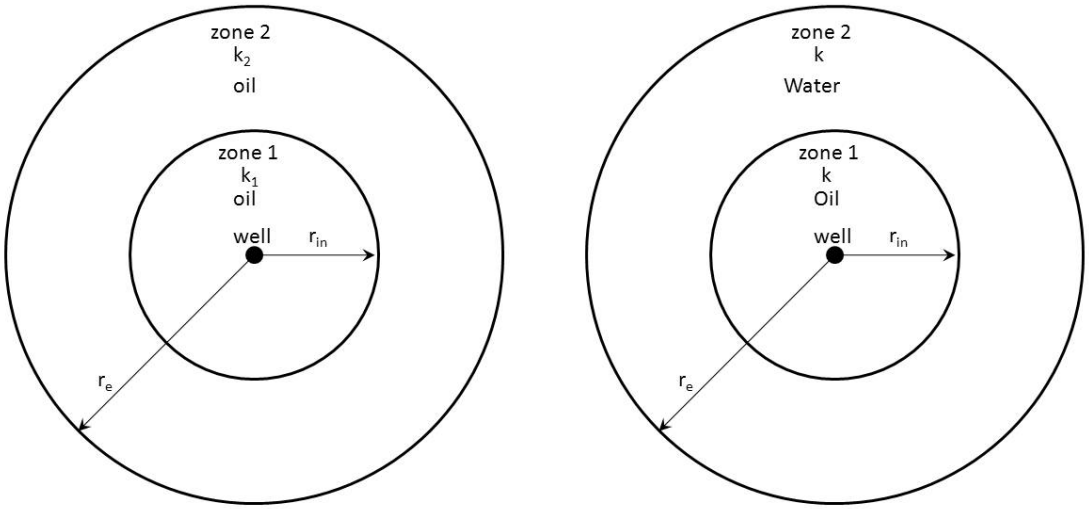

(a) (b)

Figure 3.2: Illustration of the reservoir characteristic for: a) First scenario. b) Second scenario

The first scenario involves running the model as a single phase system with two different absolute permeability zones. Analyzing the pressure transient data, a unique behavior that identifies the response at the discontinuity is expected to be observed. The second scenario involved running the model with two different fluids for each zone, oil and water, and the formation absolute permeability is kept the same in both zones. Two different cases are studied in the second scenario; i) oil in the inner zone and water in the outer zone, and ii) water in the inner zone and oil in the outer zone.

3.2 Numerical Model Validation

The first step after building the model was to validate it. The verification was undertaken by comparing the numerical model with the analytical solution for a composite reservoir. The analytical solution was developed by *Satman et al. (1980)*. The following assumptions were considered:

- The formation is horizontal, of uniform thickness, and homogeneous.
- The front is of infinitesimal thickness in the radial direction.

- The region behind the front contains only gas, while there is restricted gas flow in the region ahead of the front. However, the mobility of the gas is so much greater than that of the liquid phases that only gas flow needs to be considered.
- Flow is radial, and gravity and capillarity effects are negligible.
- The front can be considered stationary throughout the few hours of the testing period.
- The fluids are slightly compressible.

The diffusivity equations in dimensionless form for the two regions are:
For zone 1,

$$\frac{1}{r_D}\frac{\partial}{\partial r_D}[r_D\frac{\partial P_{D1}}{\partial r_D}] = \frac{\partial P_{D1}}{\partial t_D}, 1 \leq r_D \leq R_D \tag{3.1}$$

and for zone 2,

$$\frac{1}{r_D}\frac{\partial}{\partial r_D}[r_D\frac{\partial P_{D2}}{\partial r_D}] = \eta\frac{\partial P_{D2}}{\partial t_D}, R_D \leq r_D < \infty. \tag{3.2}$$

Inner boundary conditions are:

$$C_D\frac{dP_{wD}}{dt_D} - [\frac{\partial P_{D1}}{\partial r_D}]_{r_D=1} = 1 \tag{3.3}$$

and

$$P_{wD} = P_{D1} - S[\frac{\partial P_{D1}}{\partial r_D}]_{r_D=1} = 1. \tag{3.4}$$

Initial conditions are

$$P_{D1}(r_D, 0) = 0; 1 \leq r_D \leq R_D \tag{3.5}$$

and

$$P_{D2}(r_D, 0) = 0; R_D \leq r_D < \infty. \tag{3.6}$$

Conditions at the interface are

$$P_{D1}(R_D, t_D) = P_{D2}(R_D, t_D) \tag{3.7}$$

and

$$\frac{\partial P_{D2}}{\partial r_D} = \lambda \frac{\partial P_{D1}}{\partial r_D}; r_D = R_D, \, and \, t_D > 0. \tag{3.8}$$

The outer boundary condition is given as:

$$\lim_{r_D \to \infty} P_{D2}(r_D, t_D) = 0. \tag{3.9}$$

The solution in the Laplace space in terms of the Bessel functions is as follows,

$$\bar{P}_{D1}(r_D, s) = C_1 I_0(r_D\sqrt{s}) + C_2 K_0(r_D\sqrt{s}), 1 \leq r_D \leq R_D \tag{3.10}$$

$$\bar{P}_{D2}(r_D, s) = C_3 K_0(r_D\sqrt{s\eta}), R_D \leq r_D < \infty \tag{3.11}$$

$$\bar{P}_{wD}(s) = C_1[I_0(\sqrt{s}) - S\sqrt{s}I_1(\sqrt{s})] + C_2[K_0(\sqrt{s}) + S\sqrt{s}K_1(\sqrt{s})]. \tag{3.12}$$

The constants C_1, C_2, and C_3 are obtained by solving the following system of equations,

$$\alpha_{11}C_1 + \alpha_{12}C_2 = \frac{1}{2} \tag{3.13}$$

$$\alpha_{21}C_1 + \alpha_{22}C_2 + \alpha_{23}C_3 = 0 \tag{3.14}$$

$$\alpha_{31}C_1 + \alpha_{32}C_2 + \alpha_{33}C_3 = 0 \tag{3.15}$$

where

$$\alpha_{11} = C_D s[I_0(\sqrt{s}) - S\sqrt{s}I_1(\sqrt{s})] - \sqrt{s}I_1(\sqrt{s}) \tag{3.16}$$

$$\alpha_{12} = C_D s[K_0(\sqrt{s}) - S\sqrt{s}K_1(\sqrt{s})] - \sqrt{s}k_1(\sqrt{s}) \tag{3.17}$$

$$\alpha_{21} = I_0(R_D\sqrt{s}) \tag{3.18}$$

$$\alpha_{22} = K_0(R_D\sqrt{s}) \tag{3.19}$$

$$\alpha_{23} = -K_0(R_D\sqrt{s\eta}) \tag{3.20}$$

$$\alpha_{31} = \lambda\sqrt{s}I_0(R_D\sqrt{s}) \tag{3.21}$$

$$\alpha_{32} = -\lambda\sqrt{s}K_1(R_D\sqrt{s}) \tag{3.22}$$

$$\alpha_{33} = \sqrt{s\eta}K_1(R_D\sqrt{s\eta}) \tag{3.23}$$

$$\eta = \frac{(k/\phi\mu c_t)_1}{(k/\phi\mu c_t)_2} \tag{3.24}$$

$$\lambda = \frac{(k/\mu)_1}{(k/\mu)_2} \tag{3.25}$$

$$r_D = \frac{r}{r_w} \tag{3.26}$$

$$R_D = \frac{R}{r_w} \tag{3.27}$$

$$t_D = 0.0002637 \times \frac{k_1 t}{\phi_1 \mu_1 c_{t1} r_w^2} \tag{3.28}$$

$$C_D = 5.615 \times \frac{C}{2\pi\phi_1 h c_{t1} r_w^2} \tag{3.29}$$

$$P_{D1} = 0.001127 \times \frac{2\pi k_1 h}{qB\mu_1}(p_i - p_1) \tag{3.30}$$

$$P_{D2} = 0.001127 \times \frac{2\pi k_1 h}{qB\mu_1}(p_i - p_2) \tag{3.31}$$

$$P_{wD} = 0.001127 \times \frac{2\pi k_1 h}{qB\mu_1}(p_i - p_w). \tag{3.32}$$

The solution in Laplace space is then brought to the real space by numerical inversion using the Stehfest algorithm.

Fig 3.3 shows an excellent agreement between the analytical solution and the numerical simulation.

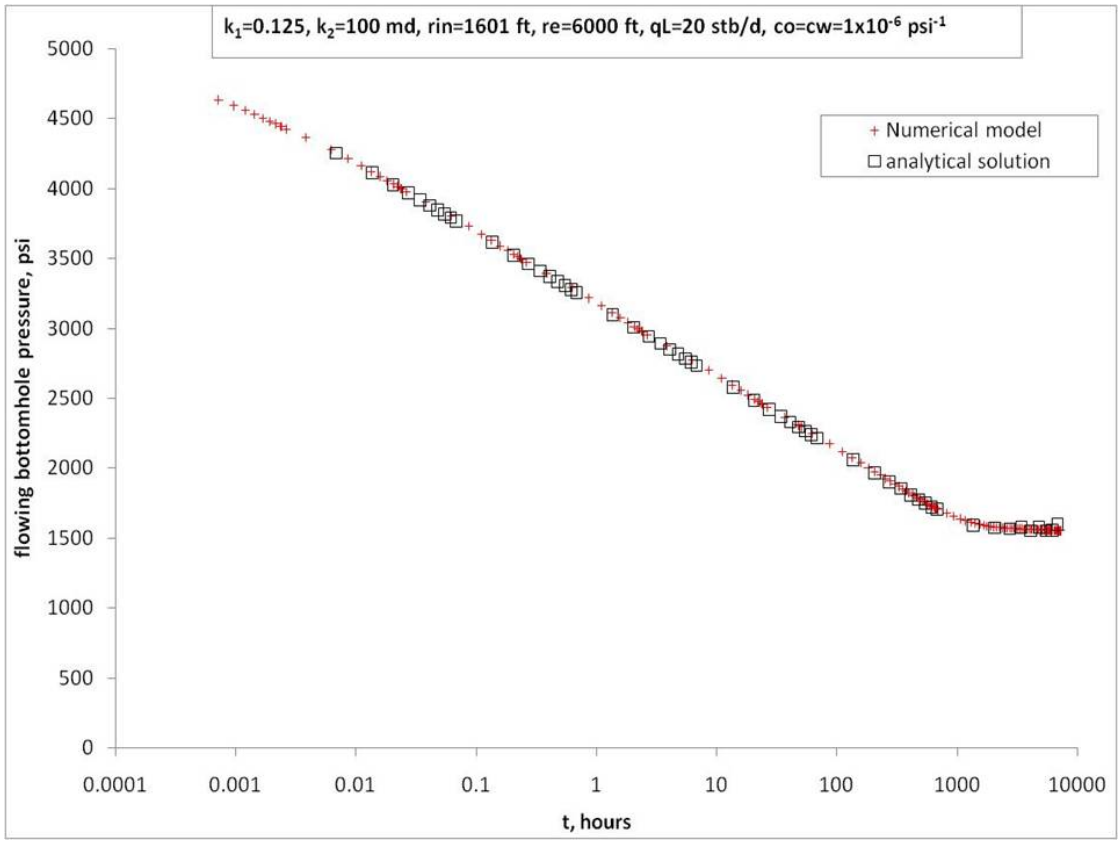

Figure 3.3: Comparison of the numerical model and the analytical solution for a composite reservoir

3.3 Results and Discussion

3.3.1 First Scenario

The model is run for two cases. Case one is the study of low permeability in the inner zone, while case two considers high permeability in the inner zone. For all the runs, pressure vs. Horner time ratio and the pressure derivative vs. equivalent time (Δt_e) were plotted.

The pressure derivative for pressure buildup is calculated using the algorithm suggested by *Bourdet et al. (1989)*,

$$\frac{d\Delta p_{ws}}{d\Delta t_e} = \frac{A+B}{C} \tag{3.33}$$

where

$$A = [\frac{\Delta p_{ws2} - \Delta p_{ws1}}{log\Delta t_{e2} - log\Delta t_{e1}}](log\Delta t_{e3} - log\Delta t_{e2}) \tag{3.34}$$

$$B = [\frac{\Delta p_{ws3} - \Delta p_{ws2}}{log\Delta t_{e3} - log\Delta t_{e2}}](log\Delta t_{e2} - log\Delta t_{e1}) \tag{3.35}$$

$$C = (log\Delta t_{e3} - log\Delta t_{e1}) \tag{3.36}$$

and Δt_e is the equivalent time, and it is calculated as follows:

$$\Delta t_e = \frac{t_p \Delta t}{t_p + \Delta t} = \frac{\Delta t}{1 + \frac{\Delta t}{t_p}} \tag{3.37}$$

In the above equation, t_p is the producing time prior to shut-in.

For the drawdown test, the pressure derivative is calculated by replacing Δp_{ws} with Δp_{wf} and replacing Δt_e with t in Eq 3.33.

Pressure plots and pressure derivative plots for the composite system with different inner and outer zone permeabilities are shown in Fig 3.4 and Fig 3.5, respectively.

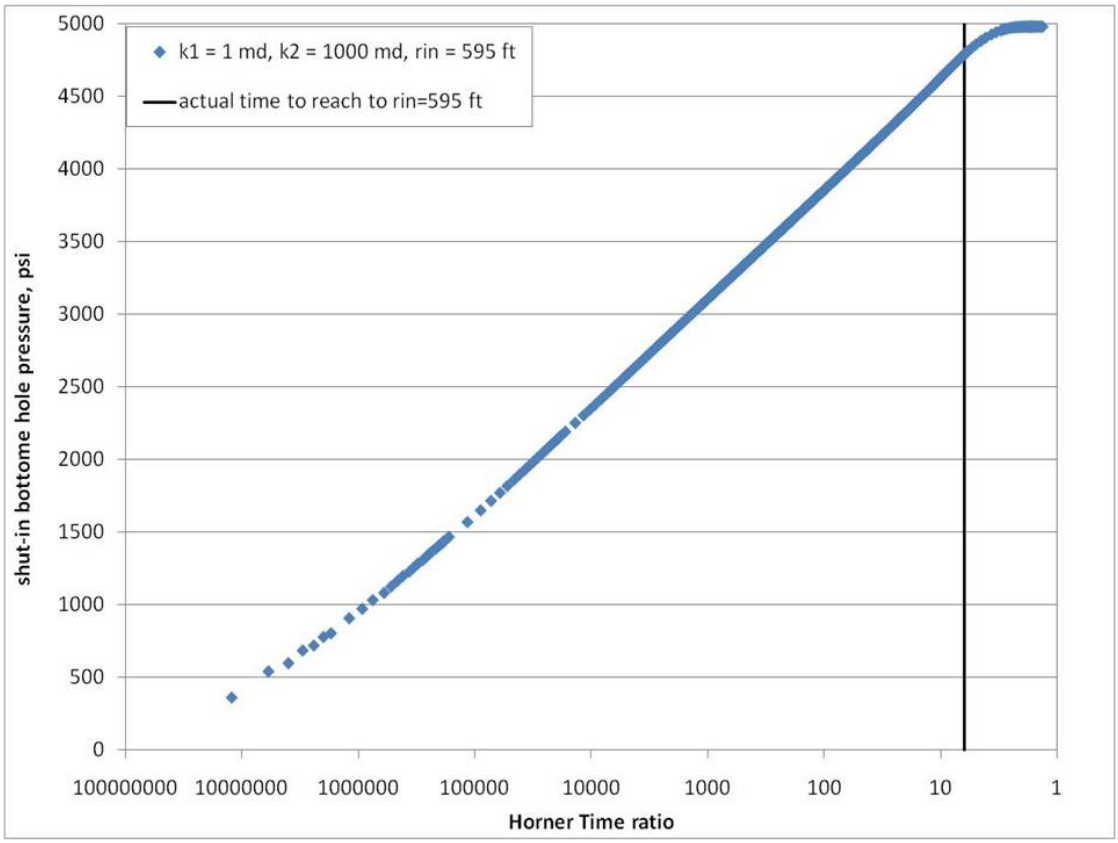

Figure 3.4: Horner plot for a composite reservoir with the smaller permeability in the inner zone

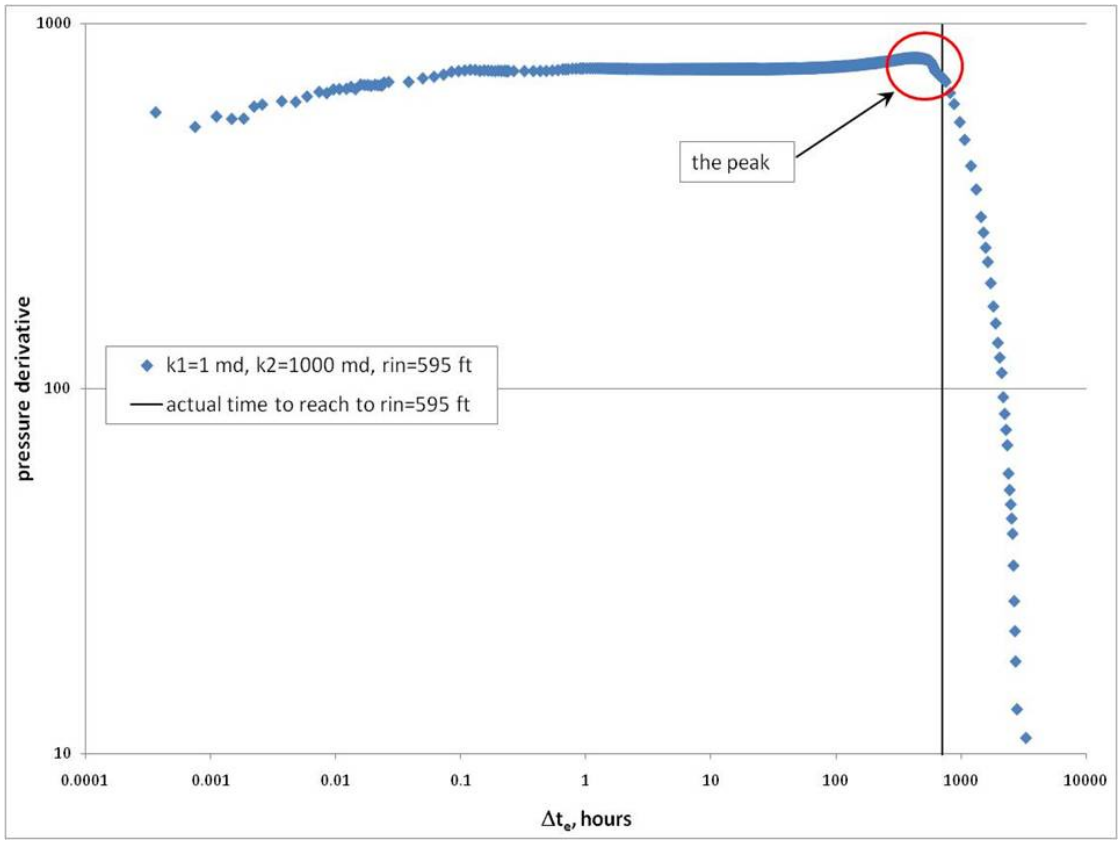

Figure 3.5: Log-log plot of pressure derivative for a composite reservoir with the smaller permeability in the inner zone

The plots of the pressure derivative for the buildup data exhibit a peak which is displayed at the end of the horizontal line representing the infinite acting period. This peak appears before the pressure derivative tends towards zero (Fig 3.5). The peak reflects the transition period between the two zones. The reason for the pressure derivative to exhibit a peak is that the pressure transient is traveling from the low mobility zone to the high mobility zone at the discontinuity, and because the flow rate is the same at the discontinuity, the pressure drop in the lower mobility zone needs to increase to deliver the same flow rate that is delivered from the higher mobility zone. On the higher mobility zone, the pressure drop needs to be decreased to deliver the same flow rate which is delivered from the lower mobility zone.

The pressure derivative for a composite system should show two horizontal lines representing characteristics of the two zones, but in Fig 3.5 there is only one horizontal line representing the inner zone. The second horizontal line is not observed or did not develop because of three reasons [*Ambastha and Ramey (1989)*]:

1. The reservoir is not large enough as the (r_e/r_{in}) ratio needs to be very large (see Fig 3.6). *Ambastha and Ramey (1989)* suggested the following condition to observe the second horizontal line in the pressure derivative:

$$\frac{r_e}{r_{in}} > \sqrt{450[1 + log(F_S)]F_S} \tag{3.38}$$

   where F_S is the storativity ratio defined as

$$F_S = \frac{(\phi c_t)_1}{(\phi c_t)_2}. \tag{3.39}$$

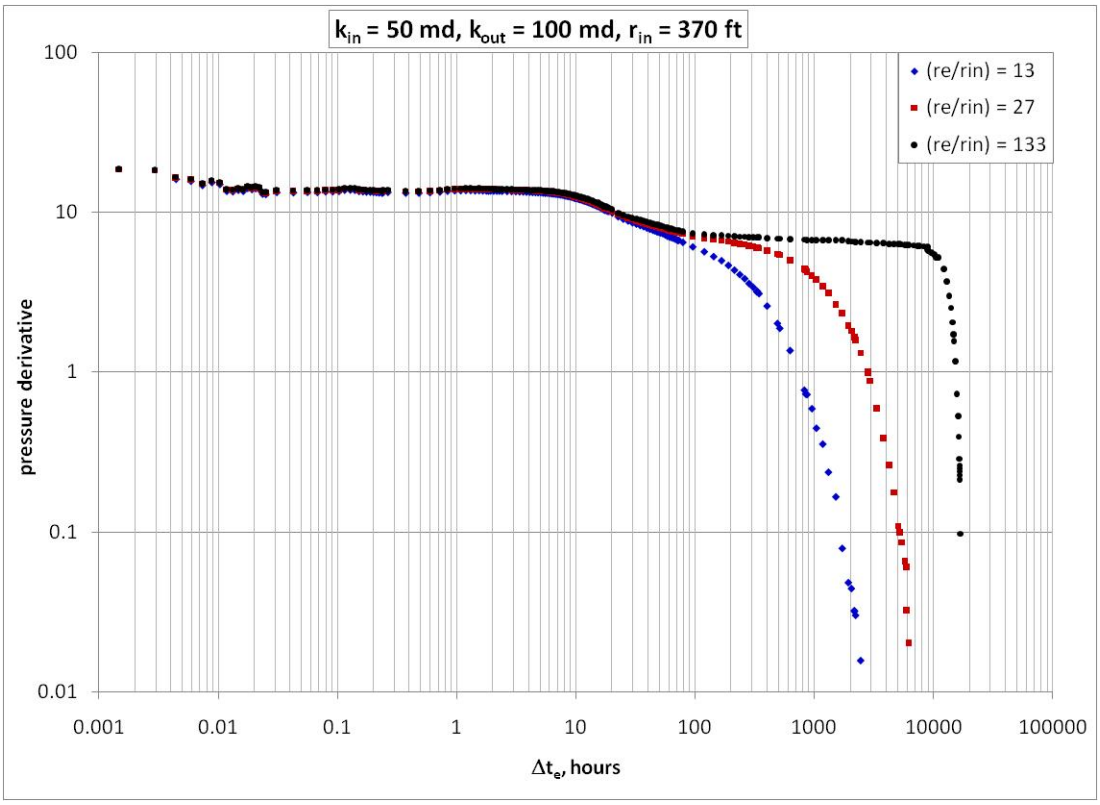

Figure 3.6: Effect of the composite reservoir's size on the development of the second horizontal line in pressure derivative plot

2. The outer boundary effects could mask the second horizontal line.

3. The transition period is so long which requires the well test to run for a long enough time to observe the second line.

This peak in many plots takes place at a time which can be used in calculating the distance to the discontinuity. The peak is clearly observed in most cases and in some cases it is not easily recognizable (Fig 3.7).

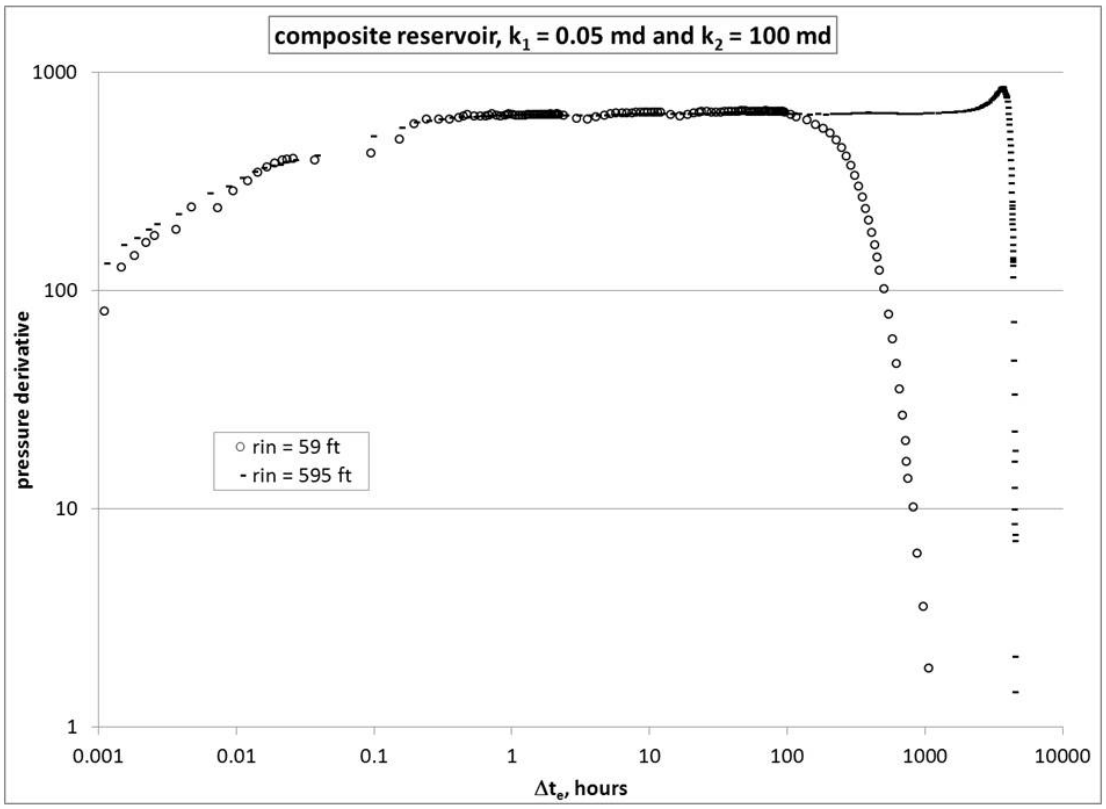

Figure 3.7: Pressure derivative for two cases and the peak is noted explicitly

This study aims at verifying if there is a relation between r_{in} and the peak. The time at the peak ($t_{(peak)}$) of the pressure derivative is used to calculate the radius of investigation from the following equation:

$$r_{inv} = \sqrt{\frac{k\Delta t}{948\phi\mu c_t}}. \tag{3.40}$$

In order to remove any confusion and to relate the names of the parameters to our study, r_{inv} will be changed to $r_{(peak)}$ and Δt to $t_{(peak)}$. Then Eq (3.40) will change to

$$r_{(peak)} = \sqrt{\frac{kt_{(peak)}}{948\phi\mu c_t}}. \tag{3.41}$$

$r_{(peak)}$ was compared to r_{in} by calculating the absolute error percentage as follows:

$$Error(\%) = \frac{|r_{in} - r_{(peak)}|}{r_{in}} \times 100. \tag{3.42}$$

Also, Eq (3.40) was re-arranged to solve for t_{in}, as follows:

$$t_{in} = 948\frac{r_{in}^2 \phi \mu c_t}{k}. \tag{3.43}$$

The previous procedures were repeated for different permeability combinations and the results are shown in Table 3.2.

Table 3.2: The different permeability combinations used with the corresponding percentage error

	r_{in}	k_1	k_2	$t_{(peak)}$	$r_{(peak)}$	Error
	ft	md	md	Hours	ft	%
1	59	0.01	1,000	528	47.2	20
2	59	0.05	100	109.13	47.98	18.67
3	59	1	100	5.5	48.17	18.40
4	59	1	1,000	5.5	48.17	18.40
5	59	10	1,000	0.18055	27.6	53.22
6	221	0.01	1,000	15,120	252.58	14.30
7	221	0.05	1,000	1,968	203.76	7.80
8	221	0.05	100	1,968	203.76	7.80
9	221	0.05	10	1,968	203.76	7.80
10	221	0.1	100	804	184.18	16.66
11	221	0.1	1,000	804	184.18	16.66
12	221	0.5	100	133.94	168.1	23.94
13	221	0.5	1,000	133.94	168.1	23.94
14	221	1	1,000	71.127	173.24	21.61
15	221	1	100	71.127	173.24	21.61
16	595	0.01	1,000	109,992	681.25	14.50
17	595	0.05	100	19,680	644.35	8.29
18	595	0.05	1,000	19,680	644.35	8.29

Table 3.2: (Continued)

	r_{in}	k_1	k_2	$t_{(peak)}$	$r_{(peak)}$	Error
	ft	md	md	Hours	ft	%
19	595	0.1	1,000	9,696	639.62	7.50
20	595	0.1	100	9,696	639.62	7.50
21	595	0.5	1,000	1,200	503.15	15.44
22	595	0.5	100	1,200	503.15	15.44
23	595	0.5	10	1,200	503.15	15.44
24	595	1	1,000	504	461	22
25	595	1	10	504	461	22
26	595	10	1,000	50.31	460.72	22.57
27	1,600	0.05	100	81,073.7	1,307.83	18.26
28	1,600	0.05	1,000	81,073.7	1,307.83	18.26
29	1,600	0.1	100	81,792	1,857.72	16.11
30	1,600	0.1	1,000	81,792	1,857.72	16.11
31	1,600	0.5	100	14,040	1,721	7.57
32	1,600	0.5	1,000	14,040	1,721	7.57
33	1,600	1	1,000	6,072	1,600.63	1.80
34	1,600	1	100	6,120	1,606.9	1.80
35	1,600	10	1,000	314.4	1,151.8	28
36	3,100	0.01	1,000	3,204,768	3,677.26	18.62
37	3,100	0.05	100	466,704	3,137.85	1.22
38	3,100	0.1	1,000	234,144	3,143.17	1.39
39	3,100	0.5	1,000	44,400	3,060.57	1.27
40	3,100	1	1,000	23,280	3,134.13	1.10
41	3,100	5	1,000	3,336	2,652.9	14.42
42	3,100	10	100	1,296	2,338.45	24.60

Table 3.2 shows that the percentage error for $r_{in} = 59$ ft is always greater than 18% unlike the other cases with longer distances, where the percentage error sometimes is less than 10%. This observation is attributed to that short distance as the pressure transient travels faster through smaller areas, and the time resolution to

capture the pressure transient data is not fine enough to show the details of the pressure transient behavior, and show the time for the peak accurately.
For all the r_{in} values, the percentage error goes through a minimum (Fig 3.8). The table also shows that chaning k_2 does not affect the error . For r_{in} = 3,100 ft, the error goes through a minimum, but the minimum occurs for more than one value of k_1. In general, for all r_{in} values for a given t_p value, the error goes through a minimum for all the different values of k_1 as displayed in Fig 3.8.

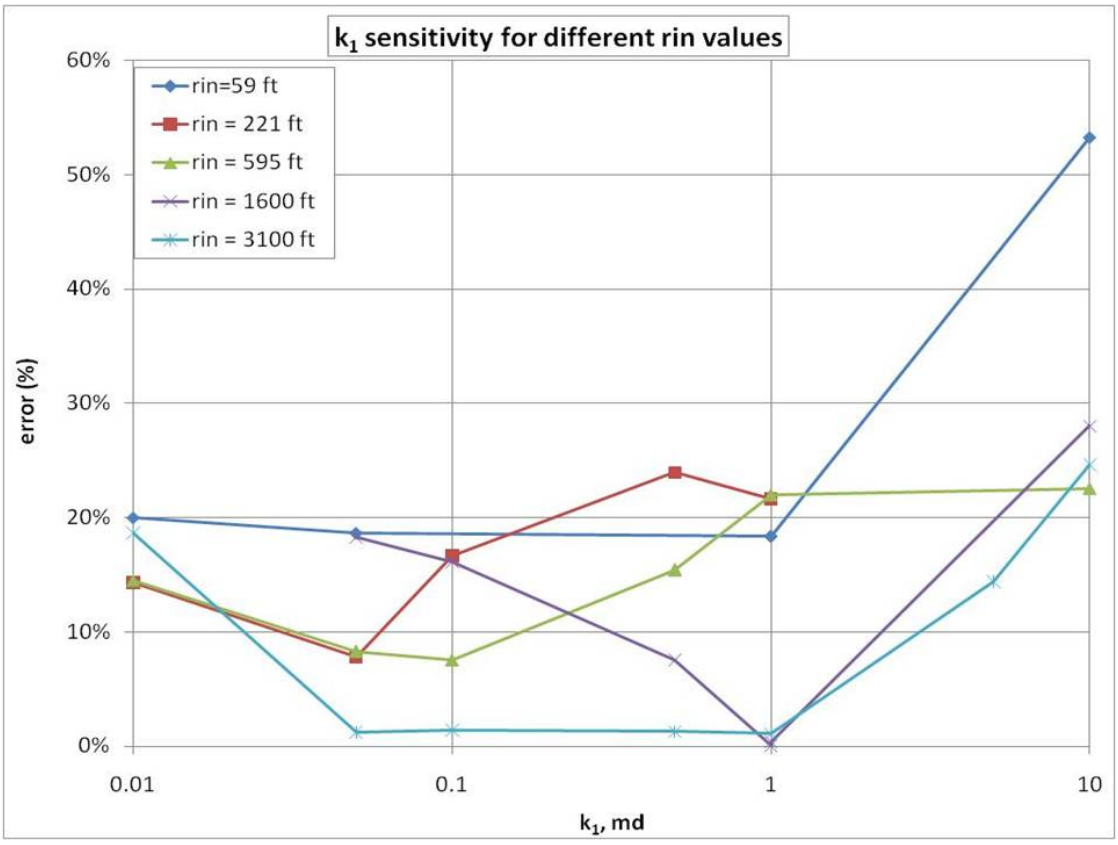

Figure 3.8: Generated errors in calculating $r_{(peak)}$ for different r_{in} and different k_1 using pressure buildup test data (t_p = 184 days).

For all the previous simulation runs, the buildup test was performed after a producing time (t_p) of 184 days (4416 hours). A sensitivity test was run to study the effect of t_p on the estimated t_{in}. Fig 3.9 and Fig 3.10 show the results of this sensitivity study.

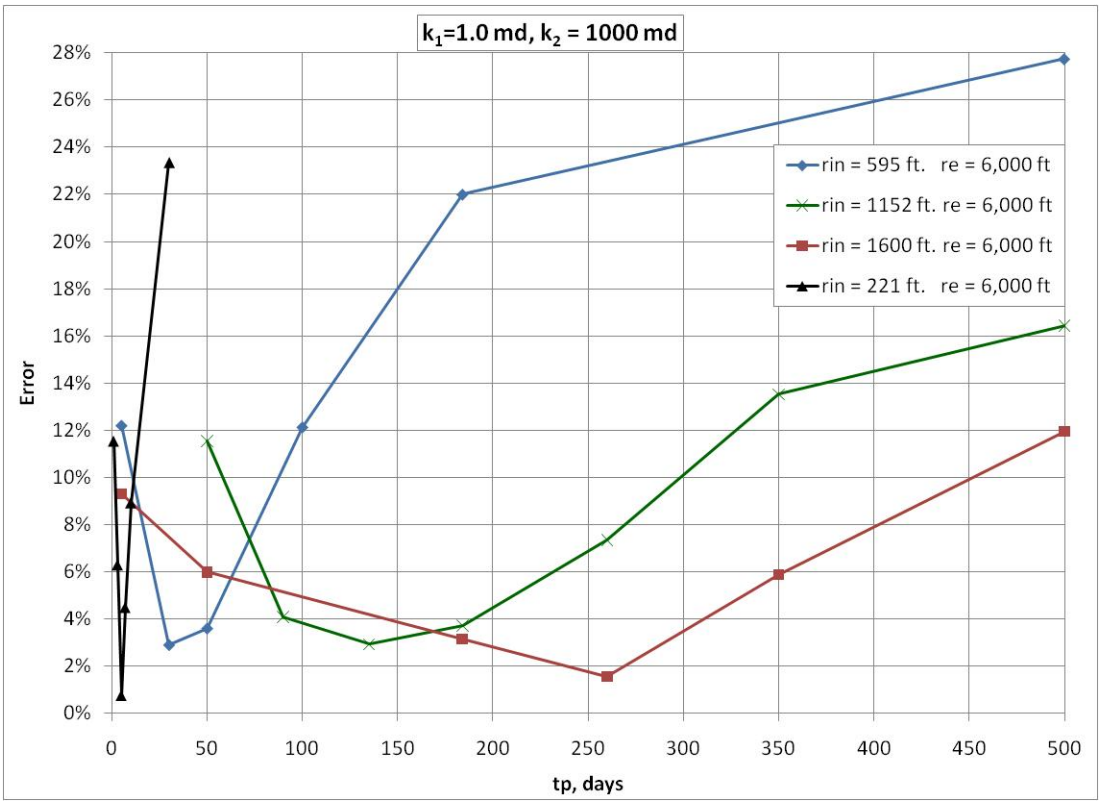

Figure 3.9: Error resulting from changing the t_p for the buildup test for different r_{in}.

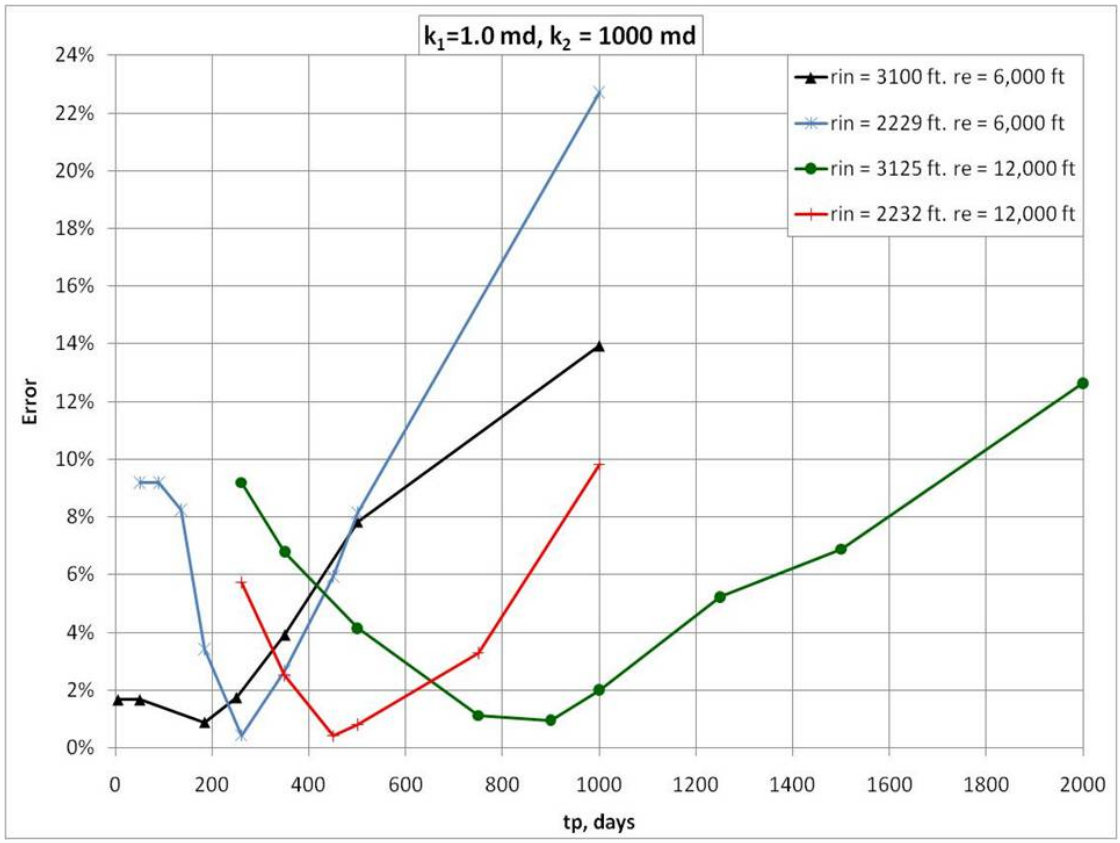

Figure 3.10: Error resulting from changing the t_p for the buildup test for different r_{in} and r_e.

Fig 3.9 shows that the error goes through a minimum at a certain t_p value. For 221 ft, 595 ft, 1,152 ft, and 1,600 ft, the minimum error occurs at a t_p value close to the value of t_{in}.

In Fig 3.10, when r_{in} is 2,229 ft or 3,100 ft for r_e equals 6,000 ft, the minimum error is found to be at a time far from t_{in}. When r_e was increased to 12,000 ft, the minimum error was at a t_p value close to t_{in} (table 3.3). This indicates that the value of t_p required to achieve the minimum error in calculating $r_{(peak)}$, will be close to t_{in} if the (r_e/r_{in}) ratio is greater than 3.
The effect of t_p on the estimated $r_{(peak)}$ is tabulated in Table 3.3.

Table 3.3: Effect of the reservoir radius (r_e) on the minimum error for $r_{(peak)}$

No.	r_{in}	r_e	r_e/r_{in}	t_{in}	t_p with minimum error
	ft	ft		days	days
1	221	6,000	27	5	5
2	595	6,000	10	35	30
3	1,152	6,000	5.2	131	135
4	1,600	6,000	3.75	253	260
5	2,229	6,000	2.69	491	260
6	3,100	6,000	1.9	949	184
7	2,232	12,000	5.38	492	450
8	3,125	12,000	3.84	964	900

Note, t_{in} in Table 3.3 was calculated using Eq (3.43).

The behavior in Fig 3.8 is difficult to be explained, because two parameters are changing in the same time (k_1, and t_p), where for each k_1 value, there is a single value of t_p that gives a minimum error for estimating r_{peak}. The behavior observed in Fig 3.9 is due to the change in one parameter, t_p, and the reason for such a behavior can be related to the distance to where the pressure transient has reached. For t_p less than or greater than t_{in}, the pressure transient, during the flow period, moves to a distance less than r_{in}, and stops there and creates somewhat a boundary layer. The pressure buildup data will then capture this this kind of a boundary layer effect as an irregular behavior which will affect the peak by changing the time for its occurrence. If t_p equals t_{in}, the pressure drawdown stops at the same distance to the discontinuity, and the response of both effects will be at the same distance and at the same time, which will produce the most accurate estimation for r_{peak}.

In the pressure drawdown tests for the case when the smaller permeability (or the smaller mobility) is assigned for the inner zone, as shown in Fig 3.11, a unique behavior in the drawdown plots was observed. Two straight lines can be clearly seen for each case. The time when the pressure transient reaches r_{in} is at the end

of the first line and the beginning of the second line. t_{in} is indicated by the three vertical lines in the figure for the three cases.

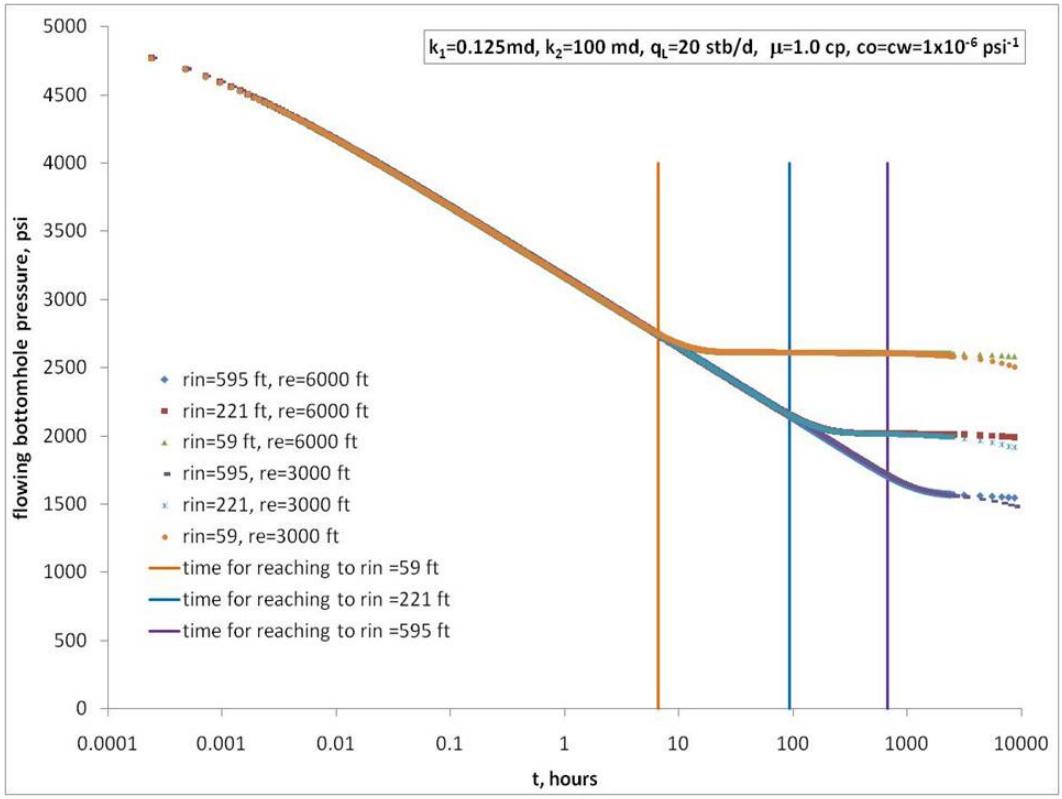

Figure 3.11: Semi-log plot for pressure drawdown for composite reservoir with the lower permeability in the inner region.

Fig 3.11 shows 6 cases; The first 3 cases for reservoirs with r_e = 6,000 ft and r_{in} equals to 595 ft for the 1^{st} case, 221 ft for the 2^{nd} case and 59 ft for the 3^{rd} case. Each of the previous 3 cases were repeated but with r_e = 3,000 ft. The figure shows a match between the cases with equal r_{in} value, except that after t = 1,000 hours, which shows the effect of the outer boundary for the cases with r_e = 3,000 ft. This proves that the second straight line is related to the outer zone.

The pressure derivative plot (Fig 3.12) shows a horizontal line and at the end of the horizontal line is the time when the pressure response reaches the discontinuity. The vertical lines indicate the time at which the pressure response reaches r_{in}. Also, the plot shows that the outer boundary has been reached by identifying the unit slope line.

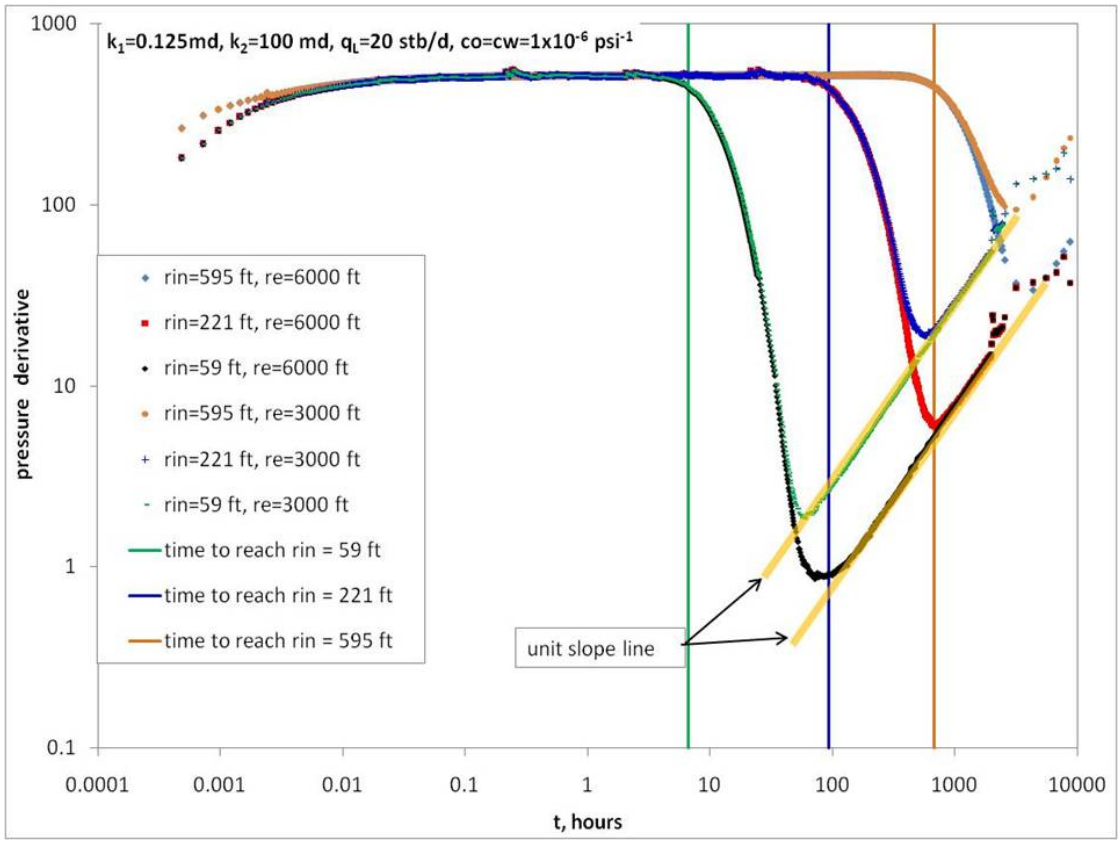

Figure 3.12: Semi-log plot for pressure derivative for composite reservoir with the smaller permeability in the inner region.

3.3.2 Second Scenario

For this scenario, single permeability was assigned to the reservoir. The model is run for four cases as follows:

Case (i) : Low viscosity oil is placed in the inner zone and high viscosity oil is placed in the outer zone.

Case (ii) : High viscosity oil is placed in the inner zone and low viscosity oil is placed in the outer zone.

Case (iii) : Water is placed in the inner zone and high viscosity oil is placed in the outer zone.

Case (iv) : High viscosity oil is placed in the inner zone and water is placed in the outer zone.

Properties of the three fluids utilized in this exercise are shown in Table 3.4.

Table 3.4: Fluid properties for the second scenario.

	water	Low Viscosity	High Viscosity
FVF (bbl/STB)	1.0	1.0	1.0
Viscosity (cp)	1.0	1.0	800
Compressibility (psi^{-1})	1×10^{-5}	1×10^{-5}	1×10^{-5}
Density (lb/ft^3)	62.4	48	48

The plot of the pressure and pressure derivative functions for cases (i) and (ii) are shown in Fig 3.13 and Fig 3.14, respectively.

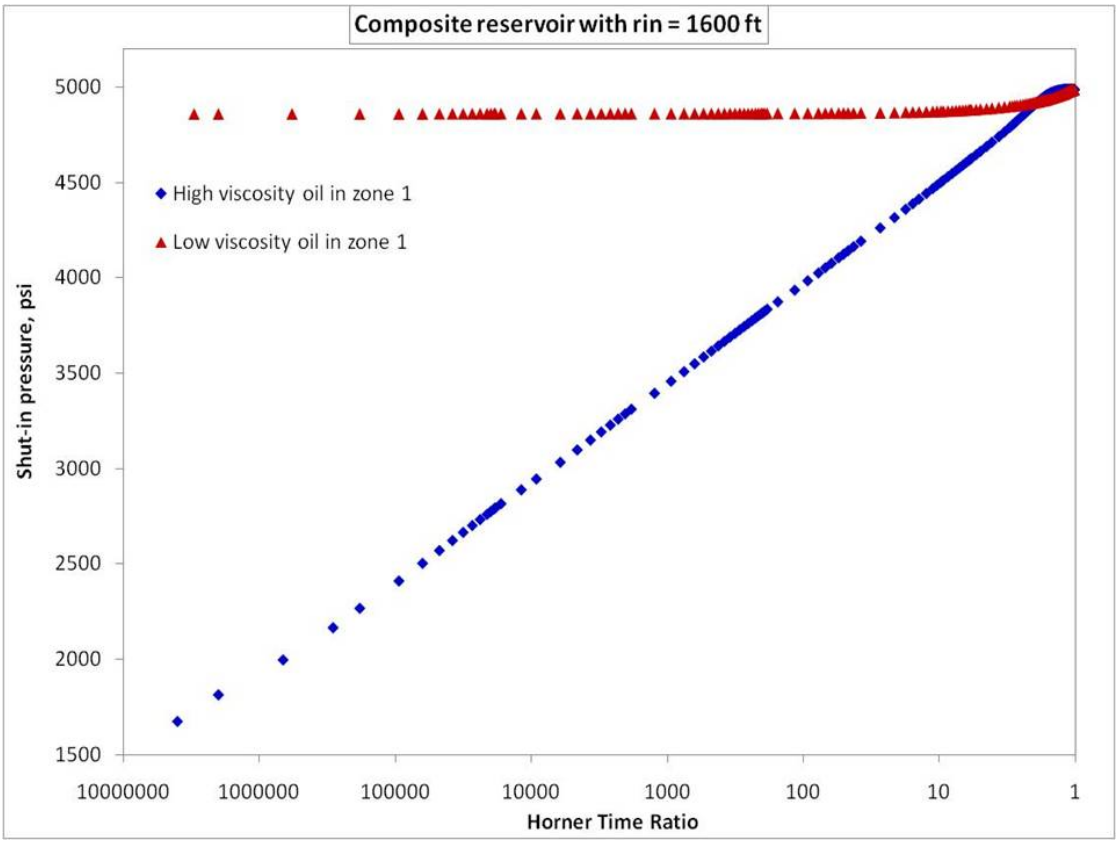

Figure 3.13: Horner plot for the second scenario for cases (i) and (ii).

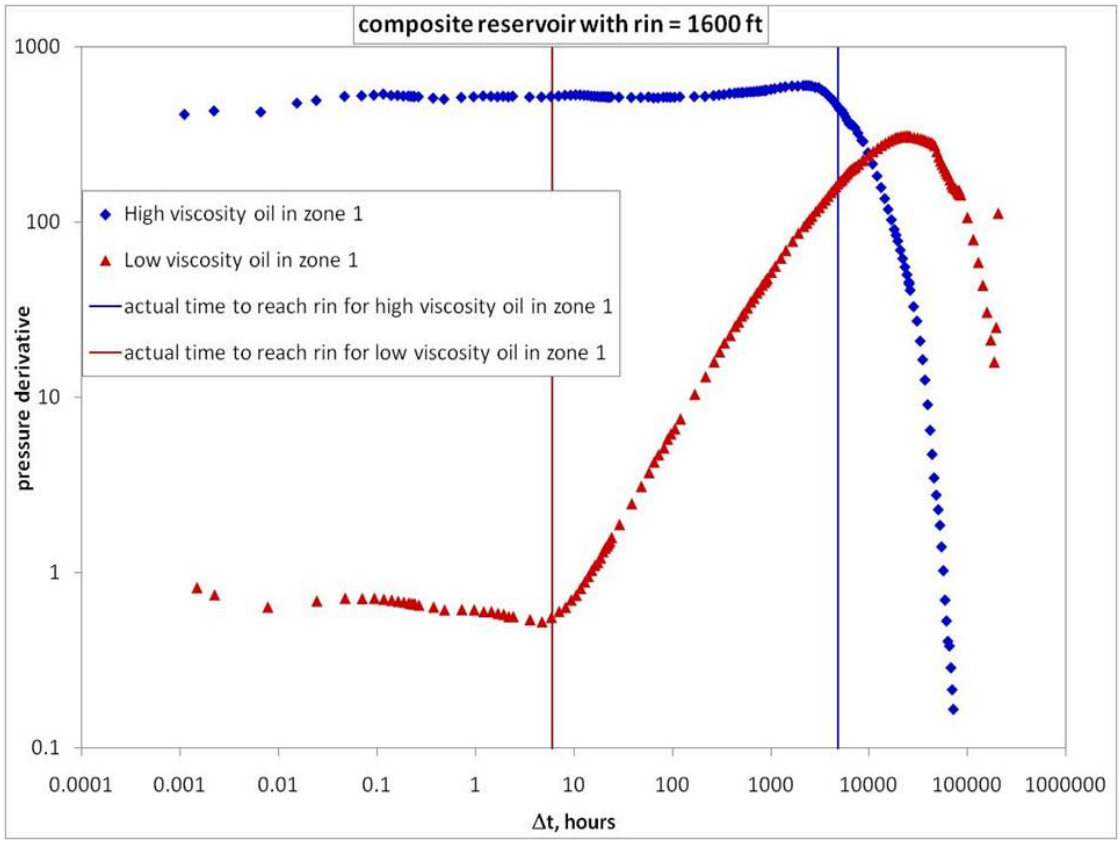

Figure 3.14: Pressure derivative plot for the second scenario for cases (i) and (ii).

For Case (i) (lower viscosity in inner zone), the behavior is different than Case (ii) and the peak is not related to r_{in} as it can be seen from Fig 3.14 where t_{in} is 6.07 hours and $t_{(peak)}$ equals to 24,408 hours. The time indicated by $t_{(peak)}$ = 24,408 hours is more related to the outer boundary.

For Case (ii) (higher viscosity in inner zone), the behavior is similar to the first scenario when the lower permeability was assigned to the inner zone. Both cases have lower mobility in the inner zone. $t_{(peak)}$ was used to calculate $r_{(peak)}$ and then the error percentage was calculated and found it to be 14.45%. Numbers of additional cases were run for different permeability and viscosity values, and the results are tabulated in Table 3.5

Table 3.5: Simulation runs for different values of permeabilities and viscosities for the second scenario (Case (ii)).

No.	r_{in}	k	μ_1	μ_2	$t_{(peak)}$	$r_{(peak)}$	Error
	ft	md	cp	cp	hours	ft	(%)
1	1,600	10	800	1	45,984	1,557	2.67
2	1,600	50	800	1	6,960	1,355	15.33
3	1,600	50	800	0.5	6,960	1,355	15.33
4	1,600	100	800	1	3,552	1,369	14.45
5	1,600	100	800	2	3,288	1,317	17.69
6	1,600	200	800	1	1,368	1,201	24.92
7	1,600	500	800	1	440.4	1,078	32.65
8	1,600	1,600	800	1	114.5	983	38.56
9	1,600	50	1,600	1	16,968	1,496	6.51
10	1,600	100	1,600	1	7,680	1,423	11.05
11	1,600	100	1,600	2	6,960	1,355	15.33
12	1,600	200	1,600	2	6,960	1,916	19.75
13	1,600	50	3,000	1	34,400	1,555	2.79
14	1,600	100	3,000	1	18,900	1,630	1.90
15	1,600	500	12,800	1	13,440	1,488	6.98
16	1,600	1,600	12,800	1	3,456	1,350	15.62
17	221	100	800	1	28.15	122	44.87
18	595	100	800	1	274	380	36.11
19	595	100	3,000	1	1,560	468	21.28
20	595	100	8,000	1	5,160	522	12.32
21	595	100	12,800	1	9,000	545	8.46
22	3,100	100	800	1	14,280	2,744	11.47

Note that we observe that as permeability increases, error increases. Another observation related to the viscosity, is that as μ_1 increases, the error decreases. In other words, as the mobility in the inner zone decreases, the error decreases. Also, as r_{in} increases, the error decreases. For cases (iii) and (iv), the results were similar to the first two cases as the comparison shown in Fig 3.15 and Fig 3.16.

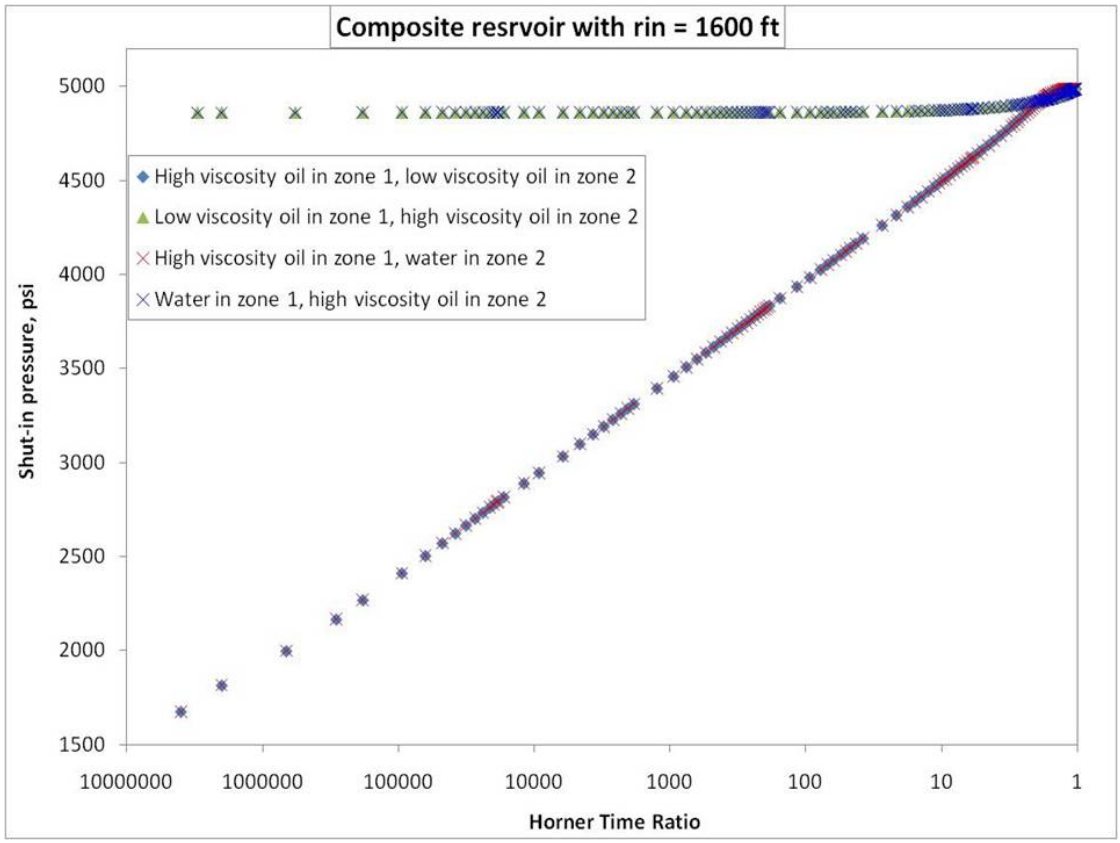

Figure 3.15: Horner plot for the second scenario for all cases.

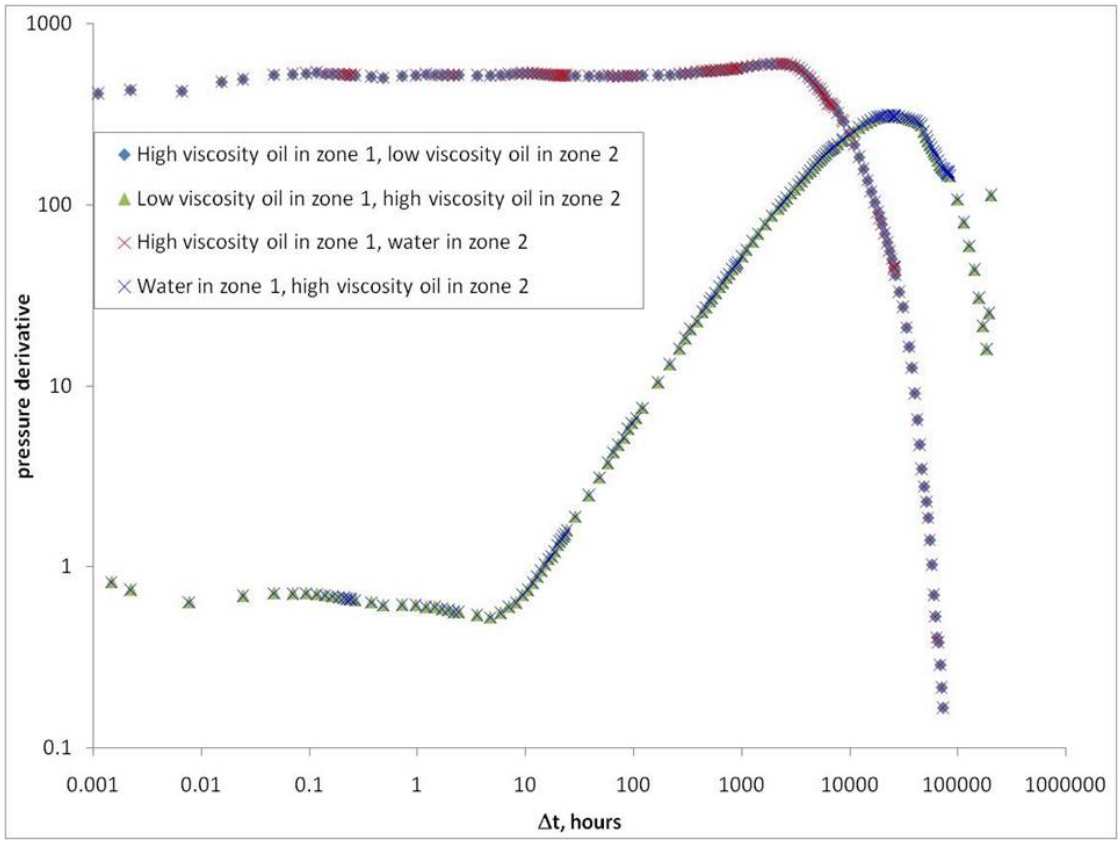

Figure 3.16: Pressure derivative plot for the second scenario for all cases.

Table 3.6 shows additional cases for reservoirs with the high viscosity oil in the inner zone and the water in the outer zone.

Table 3.6: Simulation runs for different values of permeabilities and viscosities for the second scenario (Case (iv)).

No.	r_{in}	k	μ_1	μ_2	$t_{(peak)}$	$r_{(peak)}$	Error
	ft	md	cp	cp	hours	ft	(%)
1	1,600	100	3,000	1	16,008	1,500	6.22
2	1,600	10	800	1	46,944	1,574	1.66
3	1,600	50	1,600	1	17,232	1,507	5.79
4	1,600	500	12,800	1	13,584	1,496	6.48
5	595	100	12,800	1	9,072	547	8.09
6	1,600	100	1,600	1	7,776	1,432	10.5
7	3,100	100	800	1	14,520	2,767	10.73
8	1,600	100	800	1	3,432	1,345	15.91
9	1,600	50	800	1	7,848	1,439	10.09
10	1,600	200	800	1	1,368	1,201	24.92
11	1,600	500	800	1	422	1,055	34.04

The results show that the distance to the discontinuity (r_{in}) can be estimated accurately with certain conditions. The three factors affecting the accuracy of this estimations are; r_{in}, $(k/\mu)_1$, and λ. For the reservoirs with r_{in} = 1,600 ft, the estimation is accurate if the value of $(k/\mu)_1$ is less than 0.06 and the value of λ is less than 0.00125. But for an accurate estimation for the reservoirs with $r_{in} = 595$ ft, the value of $(k/\mu)_1$ should be less than 0.007, which means as r_{in} decreases, the maximum value of $(k/\mu)_1$,which is required for accurate estimation, decreases.

Chapter 4

Water Coning Model

4.1 Models Development

4.1.1 Numerical Model

Data used to train the artificial neural networks were generated from a numerical reservoir simulation model. Two reservoir numerical models were used: radial and rectangular models. The reservoir properties are homogeneous and isotropic. In terms of fluid properties, the reservoir conditions are assumed to be above bubble-point pressure to ensure that no free gas is present in the reservoir. Furthermore, the capillary pressure was not considered. The reservoirs are horizontal with uniform thicknesses. The radial reservoir model was used to generate data for the vertical well, and the rectangular reservoir model was used to generate data for the horizontal well. The gridding for the radial system was r-θ-z, where the number of grids were 30x1x25. The thickness of all the grid blocks are equal, and the radial grids were designed according to the following equation:

$$r_i = r_w \left(\frac{r_e}{r_w} \right)^{(i/30)} . \tag{4.1}$$

The rectangular reservoir gridding was 25x25x15 and Δx = Δy = 200 ft. The reservoir properties for the radial and the rectangular systems are tabulated in the following tables.

Table 4.1: Reservoir properties for the radial system.

Porosity (ϕ)	0.25
k_r, md	500
Reservoir radius (r_e), ft	6,000
Oil formation volume factor, RB/STB	1.0
Oil compressibility (c_o), psi^{-1}	1x10^{-6}
Initial pressure (p_i), psi	5,000
Temperature, ^{o}F	130
S_{oi}	1.00

Table 4.2: Reservoir properties for the rectangular system.

Porosity (ϕ)	0.25
k_x, md	500
k_y, md	500
Reservoir length, ft	5,000
Reservoir width, ft	5,000
Oil formation volume factor, RB/STB	1.0
Oil compressibility (c_o), psi^{-1}	1x10^{-6}
Initial pressure (p_i), psi	5,000
Temperature, ^{o}F	130
S_{oi}	1.00

For the vertical well, 6 parameters were selected to be changed to create different scenarios. The parameters with their ranges are tabulated in Table 4.3.

Table 4.3: The selected reservoir properties changed within their ranges for the vertical well study.

No.	Parameter	Range
1	ρ_o, lb/ft^3	48 - 58
2	μ_o, cp	1 - 10
3	k_v, md	5 - 500
4	q_L, STB/Day	500 - 10,000
5	h, ft	25 - 250
6	h_p, ft	$0.04h$ - $0.96h$

The parameters and their ranges for the horizontal well in the rectangular reservoir are tabulated in Table 4.4.

Table 4.4: The selected reservoir properties changed within their ranges for the horizontal well study.

No.	Parameter	Range
1	ρ_o, lb/ft^3	48 - 58
2	μ_o, cp	1 - 10
3	k_v, md	5 - 500
4	q_L, STB/Day	500 - 10,000
5	h, ft	15 - 240
6	h_d, ft	$0.067h$ - $0.53h$
7	h_L, ft	600 - 3400

4.1.2 Artificial Neural Networks

4.1.2.1 Artificial Neural Networks

Artificial neural networks (ANN) are mathematical networks which are used to simulate our understanding of the biological neural networks in the human brain. When the human brain receives information from the outside environment, it will learn from it, and then make its own decisions or predictions based on the received information. The structure of the ANN is based on the structure of the neural system in the human's brain. The idea of the ANN is to have a network that can change its structure based on information fed from the outside environment. The network will learn from these information and change the structure accordingly.

The human brain contains billions of neurons that process and transmit information by chemical and electrical signals. Each neuron can send signals to many neurons and also can receive signals from many neurons and this is how the neurons are interconnected and form a network.

A simple artificial neural network consists of nodes, which can be called neurons, connected together and forming a network.

The basic structure of an artificial neural network can be explained by explaining a simple neuron model (Fig 4.1) which is the basic element of an artificial neural network.

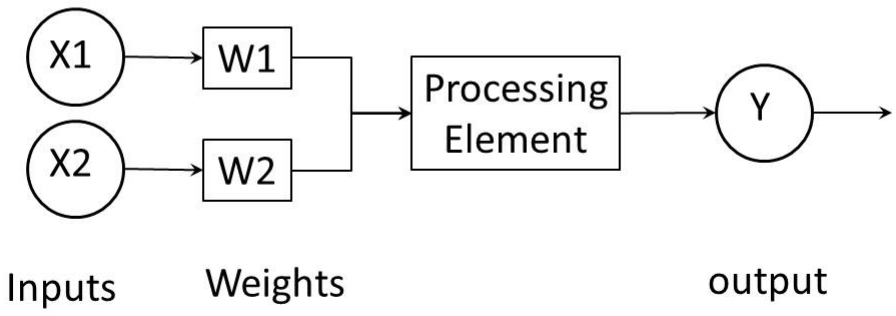

Figure 4.1: A simple model of a neuron.

Each input in Fig 4.1 is multiplied by a weighted factor, which can be adjusted according to the received information. Then, the multiplied inputs with their weights are processed through a processing element which is a transfer function, usually a non-linear function, to produce the output. This process is repeated in a process called "training" to adjust the weights and to enable the network to produce the desired output. At the beginning of the training process, the ANN will not be able to produce the desired outputs accurately, but repeating the training process results in changing the weights of the network to produce more accurate outputs, which indicates that the ANN had learned how to improve its predictions for the outputs, which is called "learning".

There are two main types of neural networks; supervised networks and unsupervised networks. The supervised networks are provided with pairs of inputs and outputs data in the training process. During the training process, the weights will be adjusted to reduce the error between the desired outputs and the neural network outputs. Unlike the supervised networks, only input data is provided for unsupervised networks. The training process of unsupervised networks will try to categorize the input data in a self-organizing behavior or try to find patterns in the input data.

There are many neural network structures, and in the petroleum industry, two types of neural networks are mainly used: 1) Feedforward multilayer perceptron network with back-propagation learning algorithm. This is the most heavily used, and 2) The self-organising network (*Ali (1994)*).

A feedforward multilayer perceptron basic structure consists of an input layer, a hidden layer and an output layer. It's called feedforward because all information flows in one direction from the input layer through the hidden layers to the output layer. Fig 4.2 shows a basic structure of a multilayer neural network with one hidden layer.

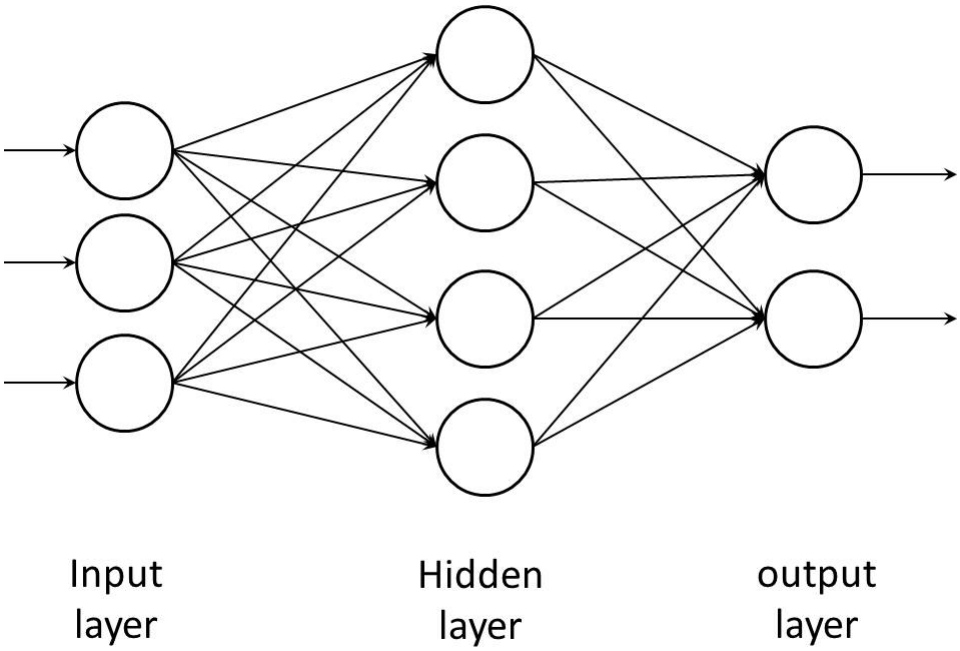

Figure 4.2: Basic structure of a multilayer neural network.

The backpropagation learning algorithm is an iterative algorithm which tries to minimize the error between the desired output and the neural network output by adjusting the weights of the network.

4.1.2.2 Vertical Well

A total of 233 combinations were generated randomly (Table A.1). Each combination was used to create a reservoir model. All the reservoir models were run using numerical simulation for 10 years. The water saturation data for all the blocks which was generated from the simulation runs was collected and prepared for the artificial neural networks training process. The artificial neural network used for training is a feedforward network, which needs inputs and outputs. The inputs are the 6 parameters in Table A.1 and the outputs are the water saturation values for all the blocks in the reservoir model at the end of each year for 10 years. The 233 reservoirs were divided into three sets; 210 reservoirs for training, 11 reservoirs for validation, and 12 reservoirs for testing. Training and validation data are used in the training of the neural network, and the testing data are only introduced to the network after the end of training process to test the new neural network.

Training the neural network started with including all water saturation values for all the blocks of each reservoir, which will produce a single network to predict the water saturation for the whole reservoir. This did not result in a good network that can predict the water saturation values with good accuracy. The next trial was to reduce the amount of data to simplify the problem for the neural network, and at the same time not produce too many neural networks. The water saturation data considered was only for one year to be used for training; if it works, this means we will have 10 different neural networks for each year. This also didn't result in a good network that can predict water saturation with good accuracy. Therefore, the amount of data was reduced more to simplify the problem by taking the data for only one layer instead of the 25 layers, but this didn't result in a good network. Then again, the data was reduced by taking the data of a single layer and considering only the 16 blocks that are closer to the wellbore. Also, with this simplification, the resulting network was not able to predict the water saturation accurately. Then, again, the number of blocks were reduced from 16 to 6 blocks. This time, a good network was generated, and the absolute error was less than 10% for all the predicted water saturation values. The absolute error is calculated using the following equation,

$$Error = |S_w - S_w(ANN)|. \tag{4.2}$$

After succeeding in designing a good network, the goal now is to increase the complexity of the problem, and reduce the number of the networks needed to predict the water saturation for the reservoir. The complexity was increased by including the data for the 10 years, and not only for one year. The produced network was good. Increasing the number of blocks to 16 blocks was tried, but did not produce a good network. The results are 25 networks, where each network predicts the water saturation for each layer at the end of each year for 10 years.

4.1.2.3 Horizontal Well

A total of 314 combinations were generated randomly (Table A.2), and for each combination, a reservoir was created. The horizontal section was always in the center in the j-direction for all the reservoirs. This created a symmetry, which will reduce the amount of data to be considered, and in return, will reduce the time needed to train the neural network. Fig 4.3 shows the *x*-*z* plane for the rectangular reservoir system for j = 13. The water saturation of the blocks in the center column will be included in the output data, and the water saturation for the blocks on both sides will be identical, and either one can be considered.

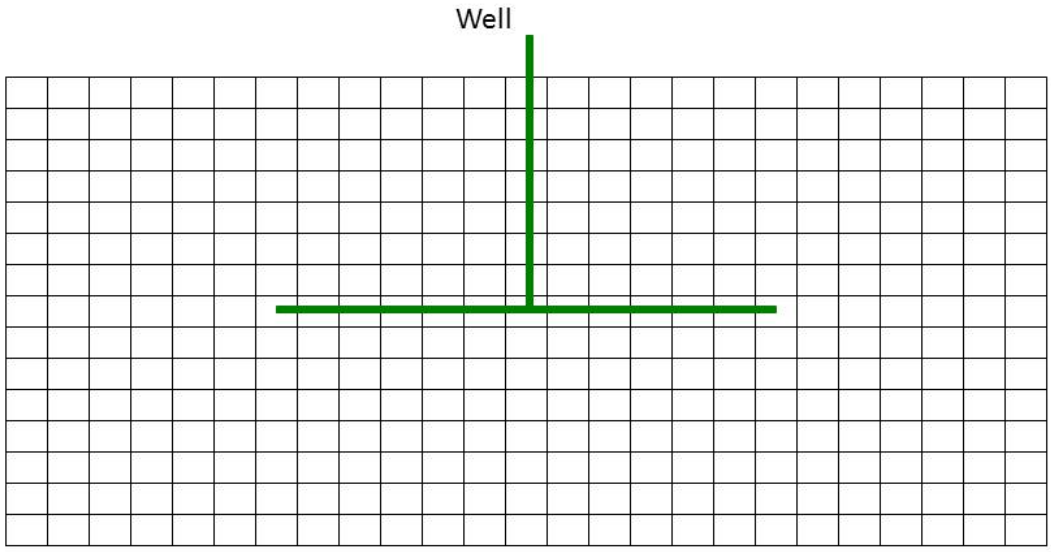

Figure 4.3: x-z plane of the rectangular reservoir system for j=13 and showing the horizontal well.

After running the numerical simulation for all the reservoirs for 10 years, water saturation data was collected and prepared for training the neural network. The data collected was only from the vertical plane which contains the horizontal well (Fig 4.3). This is done to reduce the amount of data, and hence reduce the time for training the neural network.

The water saturation for each block at the end of each year was collected. This was done for all the blocks in Fig 4.4. At the end, we had 375 blocks (25×15) to

be considered. Because of the symmetry of the reservoir, we only took the first 13 columns. Training the neural network using the water saturation values for the blocks in a single column, produced 13 different neural networks. All neural networks have the same inputs, but the difference is in the values of the water saturation, where the first neural network used the water saturation values of all the blocks in the first column for the 10 years, and the second neural network used the data for the second column, etc.

The data from the 314 reservoirs were divided into 3 sets: 284 for training, 15 for validation, and 15 for testing. The training and validation set were used in the training process, but the testing set was not introduced to the network during training process. The ANN is considered good when the predicted water saturation of the testing data has an absolute error of less than 10% for all values. Fig 4.4 shows the x-z plane of the reservoir and the numbering of the rows and columns.

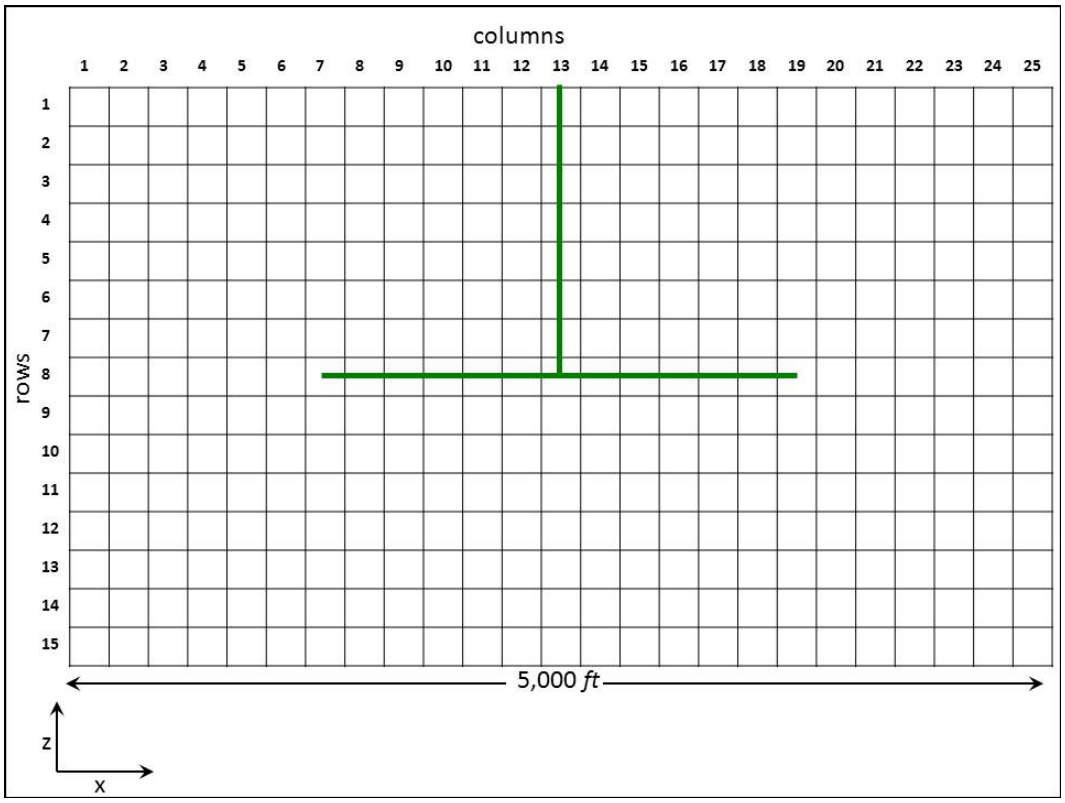

Figure 4.4: x-z plane of the reservoir for j=13 and showing the horizontal well with numbering of rows and columns.

Three approaches were used to select the best data to train the neural network:

1. Considering the water saturation data for the whole vertical plain (because of the symmetry, half of the plane was considered).

2. Considering the water saturation data for each layer.

3. Considering the water saturation data for each column. (because of the symmetry, only 13 columns were considered out of 25 columns).

Considering columns for training the neural network gave the lowest absolute error.

The first trial to train the neural network was done by using the water saturation data of the blocks in columns 1 - 13. Water saturation values of blocks in columns 14 - 25 were not included because they are identical to the values in columns 1 - 12. No good network was produced. The data then was reduced by selecting the data of a single layer to train a neural network. Starting with the first layer at the top of the reservoir, the error was very small. Moving to the second layer, the error slightly increased, but was still good, because all the predicted values had an absolute error of less than 10%. At Layer 6, some of the blocks showed an error above 10%. Moving to the next layers, the error was increasing until Layer 14. The error for Layer 15 was lower than the previous 5 layers, but not good enough, because many blocks had an absolute error above 10%.

Then, a different approach was followed to see if better results can be produced. Instead of taking the blocks in each layer and use their water saturation values to train a neural network, the blocks in each column were considered. The columns which were considered are columns 1-13 because of the symmetry (see Fig 4.4). Training the neural network started with using the water saturation values in the blocks in Column 13, because it is the most complicated column. The greatest change in water saturation is happening in Column 13. Then moving to Column 12, until Column 1. The average absolute error of Column 1 was the minimum error, and the error increased from Column 2 to Column 13.

The structure of the artificial neural network was selected after trial and error. The network with the lowest error found was the feedforward network. The learning function with lowest error was the gradient descent with momentum weight and bias learning function. The training function with the lowest error was the conjugate gradient backpropagation with Polak-Ribiére updates. The transfer functions which showed the lowest error was the hyperbolic tangent sigmoid transfer function.

The neural network structure consists of the input and the output layers and two or more hidden layers. In each layer (input, output and hidden), the number of neurons must be specified. The number of neurons in the input layer are 7, which are the parameters in Table A.2. The number of neurons in the output layer are 150. 150 neurons are required because each column has 15 blocks, and the water saturation value for a single block was taken at the end of each year for 10 years.

Determining the number of hidden layers and neurons in a hidden layer is a trial and error process. Several training processes need to be performed with different numbers of hidden layers and neurons to reach the best structure that gives the lowest average absolute error.

4.2 Results and Discussion

4.2.1 Vertical Well

In this case, 25 artificial neural networks were created. They were tested using data from the 12 reservoirs. The average absolute error was less than 10% for the data of the layers for all 12 reservoirs. The structure of all the networks consists of one input layer, one output layer and two hidden layers. For each network, the outputs were the water saturation values for the blocks at the end of the year for the 10 years, and the inputs are 6 parameters, they are:

1. Oil density.

2. total liquid flow rate.

3. Oil viscosity.
4. Reservoir thickness.
5. Vertical permeability.
6. Open interval to the flow.

Fig 4.5 shows the structure of the generated ANN for the first layer. The network has 6 inputs in the input layer, 46 neurons in the first hidden layer, 37 neurons in the second hidden layer, and 60 outputs in the output layer.

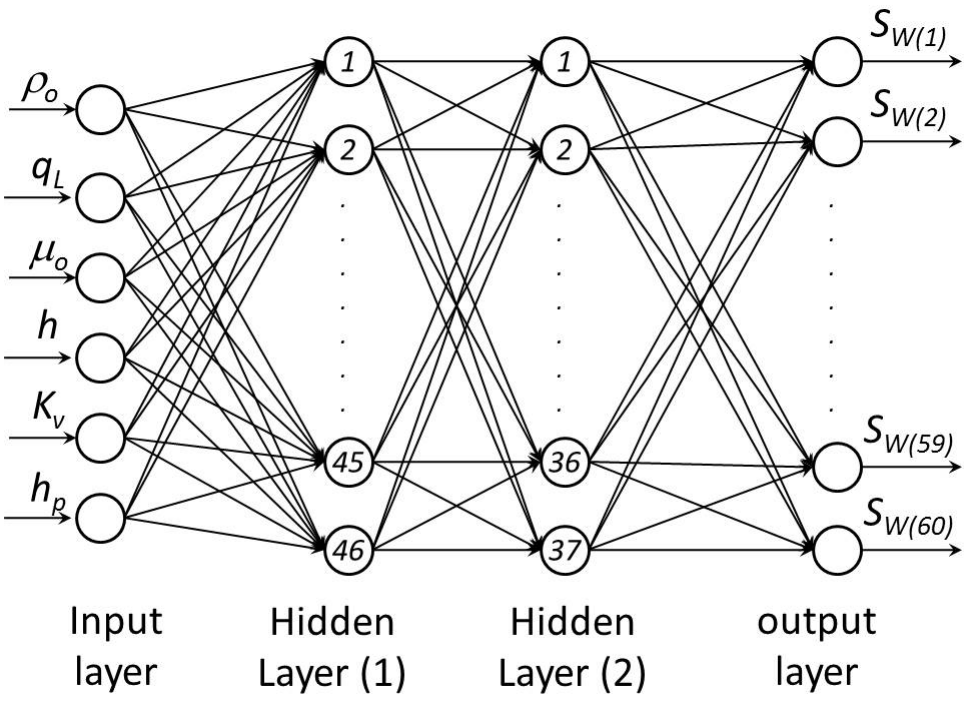

Figure 4.5: ANN structure generated for the first layer for the vertical well.

Table 4.5 shows the average absolute error for each layer for the 12 reservoirs used for testing the generated neural networks.

Table 4.5: Average absolute error for the predicted water saturation for the 12 testing reservoirs by ANN for each layer for the vertical well.

Layer No.	Average absolute Error	Layer No.	Average absolute Error
1	0.07%	14	1.03%
2	0.15%	15	1.15%
3	0.36%	16	1.67%
4	0.76%	17	1.29%
5	0.32%	18	1.52%
6	0.56%	19	1.13%
7	0.73%	20	0.95%
8	0.53%	21	0.97%
9	0.54%	22	1.04%
10	0.49%	23	0.81%
11	0.64%	24	0.80%
12	0.86%	25	0.57%
13	0.97%		

Two reservoirs (reservoir # 230 and #233) were selected, from the 12 reservoirs used to test the generated neural network, to show the behavior of the ANN in predicting the water saturation. Reservoir # 230 has the highest average absolute error, among the 12 tested reservoirs, for the predicted water saturation values, and reservoir # 233 was randomly selected. Table 4.6 shows the input parameters for the two selected reservoirs.

Table 4.6: input parameters for reservoirs # 230 and # 233.

res. #	ρ_o, lb/ft^3	q_L, STB/D	μ_o, cp	k_v, md	h_p, ft	h, ft
230	52.9	5,290	8.9	399	3.6	22.5
233	53.05	5,305	9.05	401	4.2	26.25

Fig 4.6 (a) shows the surface map of the water saturation for reservoir # 233 with numerical simulation data. Fig 4.6 (b) shows the same reservoir but with predicted data from ANN. The prediction has a very low error, and the cone shape

is developed very clearly. Fig 4.6 (c) shows the absolute error on a surface map to give a better way of visualizing the error and its location. The highest error is 5.9% and it is in a very small area. Fig 4.7 shows progress of saturation maps for the reservoir # 233 with predicted ANN data over a period of 10 years.

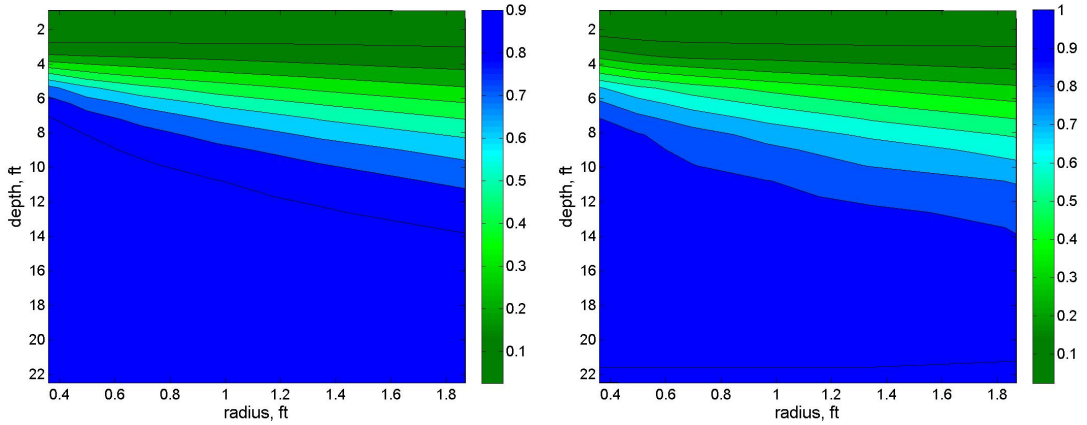

(a) Numerical simulation **(b) Artificial neural network**

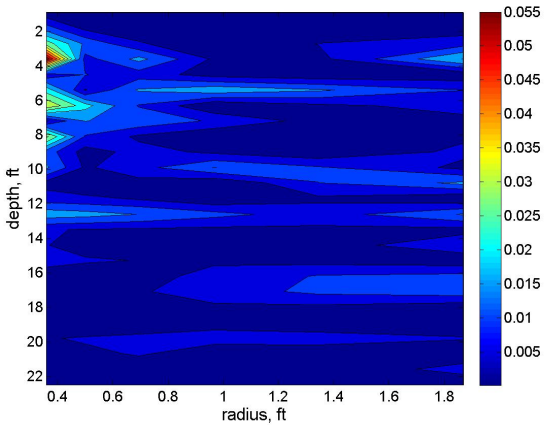

(c) Absolute error

Figure 4.6: Surface map of S_w for reservoir # 233 at the end of the 6th year.

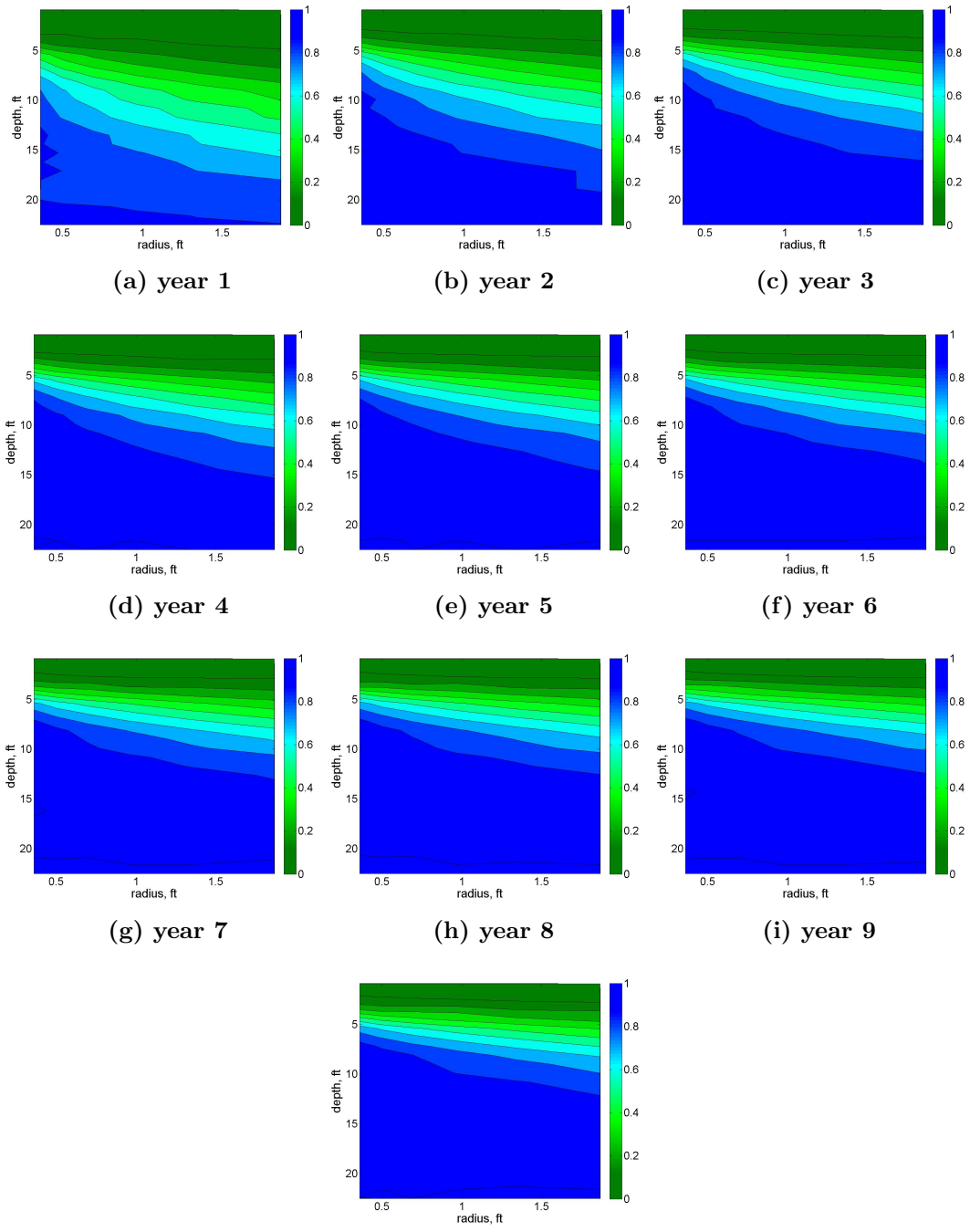

(a) year 1 **(b) year 2** **(c) year 3**

(d) year 4 **(e) year 5** **(f) year 6**

(g) year 7 **(h) year 8** **(i) year 9**

(j) year 10

Figure 4.7: Water saturation map for reservoir # 233 using ANN data.

Fig 4.8 (a) is for the surface map for reservoir # 230 for the water saturation using the data from the numerical simulation. Fig 4.8 (b) is the surface map for the

same reservoir using data predicted with the ANN. Fig 4.8 (c) shows the absolute error. Prediction for this reservoir has the highest error among the 12 reservoirs used for testing, but the shape of the cone has developed is clearly visible.

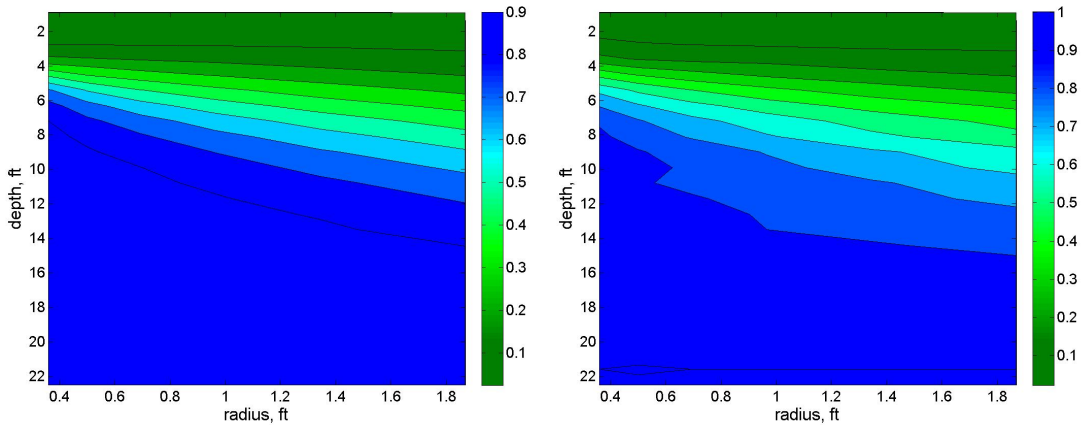

(a) Numerical simulation

(b) Artificial neural network

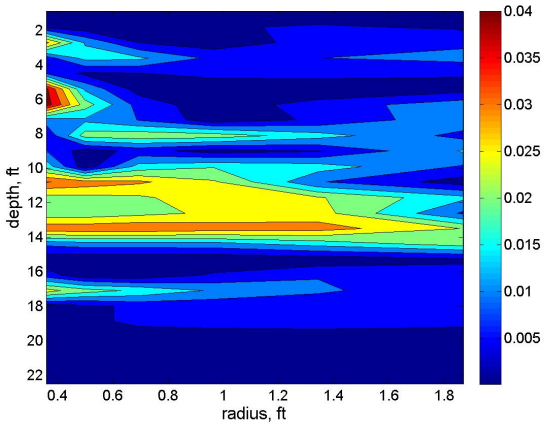

(c) Absolute error

Figure 4.8: Surface map of S_w for reservoir # 230 at the end of the 5th year.

The results for the previous two reservoirs show good predictions. The ANN show a good prediction at the areas where the water saturation is not changing, or the change is very small. The error is almost zero at the top of the reservoir, because the water saturation is not changing. Also, at the bottom of the reservoir, the error is very low, because the change of water saturation is very small. The results also show that the high values of error occur around the wellbore and in the areas

of transition saturation, because the saturation is changing at a faster rate than other locations, and it's more challenging for the ANN to predict the change in water saturation over a shorter period of time compared to other locations of the reservoir. In Appendix C, for comparison purposes, two additional case study results are presented for slow and medium moving saturation fronts.

4.2.2 Horizontal Well

13 artificial neural networks were generated. Each network predicts the water saturation for each column. The structure of all the networks consists of one input layer, one output layer and 2 or 3 or 4 hidden layers. For the output layer, the outputs were the water saturation values for the blocks at the end of the year for the 10 years. The inputs are 7 parameters, they are:

1. Oil density.
2. Total liquid flow rate.
3. Oil viscosity.
4. Reservoir thickness.
5. Vertical permeability.
6. Depth of the horizontal well.
7. Length of the horizontal well.

Fig 4.9 shows the structure of the generated ANN for the first column. The network has 7 inputs in the input layer, 31 neurons in the first hidden layer, 37 neurons in the second hidden layer, and 150 neurons in the output layer.

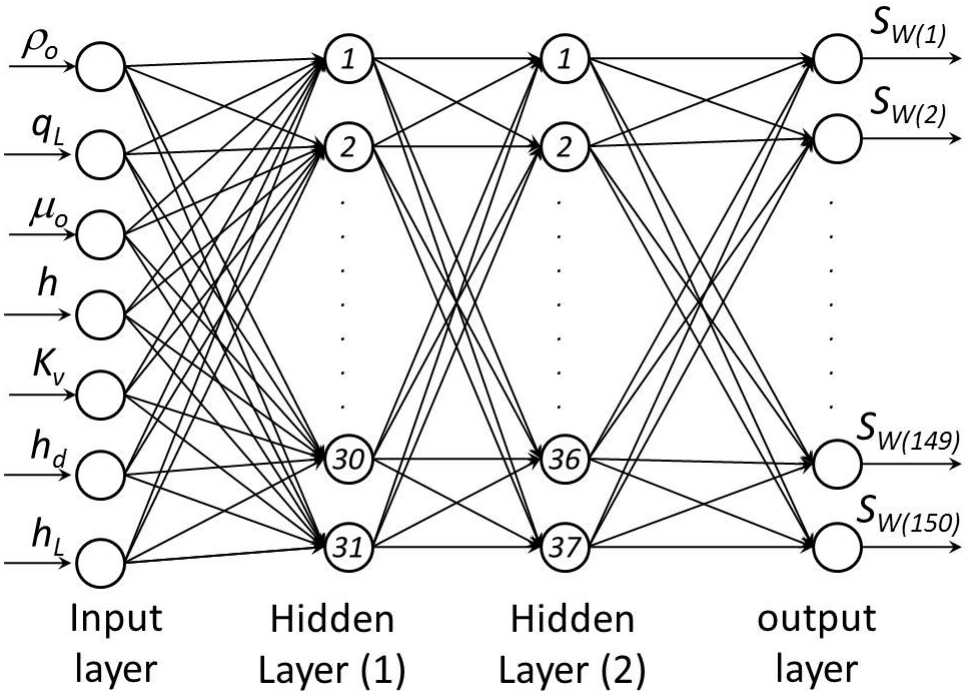

Figure 4.9: ANN structure generated for the first column for the horizontal well.

Table 4.7 shows the average absolute error for the 15 reservoirs used for testing the generated neural networks.

Table 4.7: Average absolute error for the predicted water saturation for the 15 testing reservoirs by ANN for each column for the horizontal well.

Column No.	Average absolute Error
1	0.366%
2	0.343%
3	0.341%
4	0.385%
5	0.467%
6	0.941%
7	1.072%
8	1.916%
9	2.369%
10	2.587%
11	2.403%
12	2.716%
13	1.985%

15 reservoirs were tested with the generated neural networks and two reservoirs were selected to illustrate the results of the neural network predictions. The two selected reservoirs are reservoirs # 8 and # 10 and Table 4.8 shows their input parameters.

Table 4.8: input parameters for reservoirs # 8 and # 10.

res. #	ρ_o, lb/ft^3	q_L, STB/D	μ_o, cp	k_v, md	h, ft	h_L, ft	h_d, ft
8	51.766	6,286	9.9006	253	136.47	3,400	40.942
10	50.898	5,319	2.0525	192	210.79	2,600	105.40

Fig 4.10 (a) shows the surface map for reservoir # 8 of water saturation from numerical simulation. The horizontal well is at a depth of 41 ft and the horizontal section is 3,400 ft long extending from 800 ft to 4,200 ft. Fig 4.10 (b) shows the surface map for the same reservoir with water saturation data predicted from ANN.

Fig 4.10 (c) shows the absolute error of the ANN predicted water saturation for reservoir # 8. Fig 4.11 shows progress of saturation maps for the reservoir #8 with predicted ANN data over a period of 10 years.

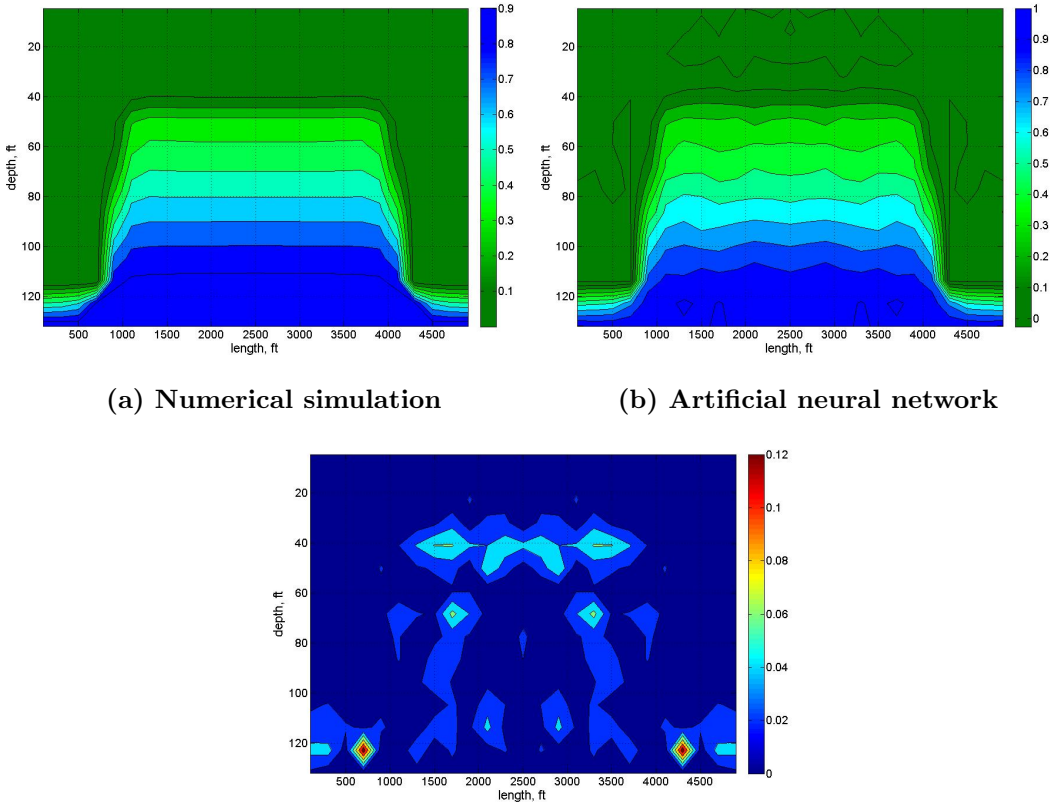

(a) Numerical simulation **(b) Artificial neural network**

(c) Absolute error

Figure 4.10: Surface map of S_w for reservoir # 8 at the end of the 10th year.

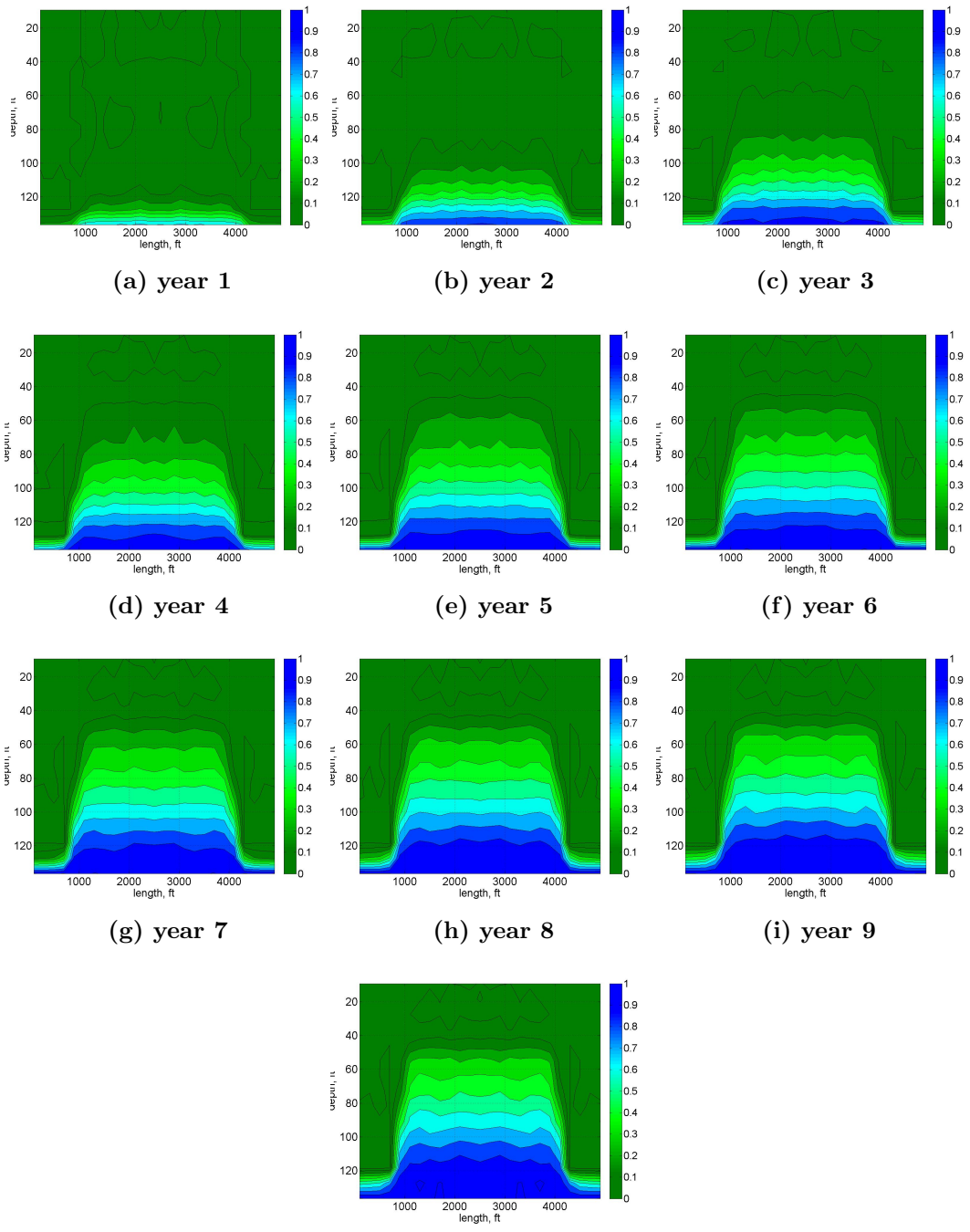

(a) year 1 **(b) year 2** **(c) year 3**

(d) year 4 **(e) year 5** **(f) year 6**

(g) year 7 **(h) year 8** **(i) year 9**

(j) year 10

Figure 4.11: Water saturation map for reservoir # 8 using ANN data.

The ANN was able to predict the shape of the cone. There are areas which show an absolute error larger than 10%, but they are at the bottom of the water cone which

is less important (Fig 4.10 (c)). The more important areas are those which show where the water front has reached. The high error zones occurs at the transition zones, similar to results for the vertical wells. The high error occurs at the transition zones because saturation gradients are high over a small area, which creates a greater challenge to the ANN to predict the water saturation values accurately.

The second example to illustrate the ability of the ANN to predict the water coning phenomena is for reservoir # 10. Fig 4.12 (a) shows the surface map of water saturation for the reservoir with the numerical simulation data, and Fig 4.12 (b) shows the surface map for the same reservoir with the ANN predicted data. The ANN was able to predict the cone shape and also to predict the sharp decrease of water saturation at the bottom sides of the cone.

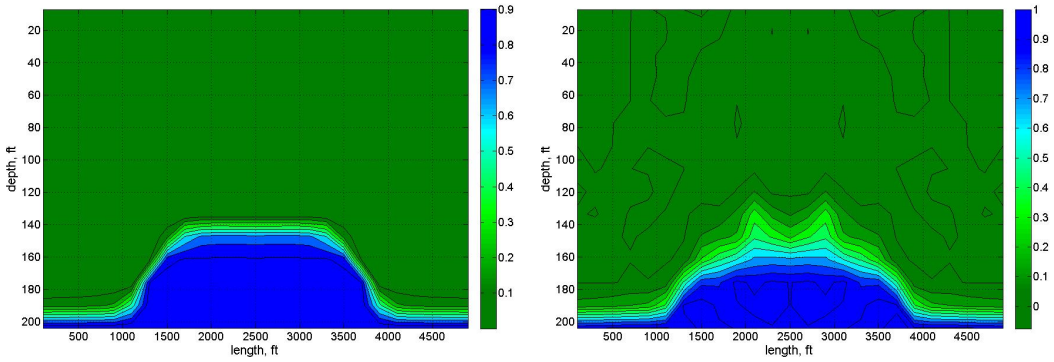

(a) Water saturation from numerical simulation

(b) Water saturation from artificial neural network

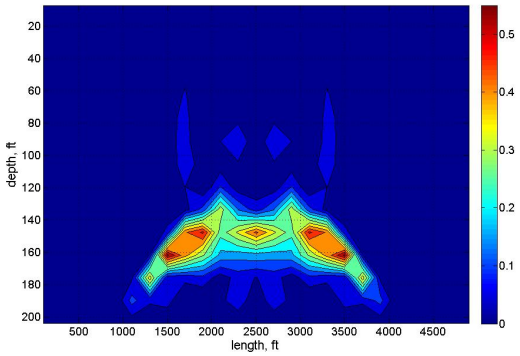

(c) Absolute error

Figure 4.12: Surface map of S_w for reservoir # 10 at the end of the 10th year.

Fig 4.12 (b) shows two identical peaks. This is an overestimate for the water saturation values and this is because the horizontal section of the well, which is off the center, is having more flow than the center section. The ANN was successful in predicting this behavior but the values for water saturation were overestimated. In Appendix D, for comparison purposes, two additional case study results are presented for slow and medium moving saturation fronts.

Chapter 5

Conclusions

This study consisted of two parts. The first parts is concerned with the use of the pressure transient data to determine the distance to the discontinuity in an oil reservoir with edge water. The reservoir is considered as a composite reservoir with the oil phase in the inner zone and the water phase in the outer zone. Some of the parameters that affect the determination of the distance to the discontinuity were studied. A procedure is proposed to help estimate the distance to the discontinuity under certain conditions. The procedure can be applied using the pressure derivative for buildup test data if the mobility ratio is less than unity. A peak must be observed in the pressure derivative curve. Looking at the highest value of the pressure derivative in the peak, and then taking the corresponding time for it and using it to calculate the radius of investigation which in this case is the distance to the discontinuity.

For a peak to be observed in a reservoir with r_{in} = 1,600 ft, the mobility of the inner zone has to be very small (less than 0.06), and also the mobility ratio has to be small (preferably less than 0.00125). Considering the previous conditions given for the mobility in the inner zone and the mobility ratio, the procedures will accurately predict the distance to the discontinuity for large distances (1,600 ft or larger), but for shorter distances, the error can be high. For the error to be low for shorter distances, the mobility for the inner zone has to be less than what it should be for r_{in} = 1,600 ft.

The second part is concerned with predicting water saturation distribution in oil reservoirs using artificial neural networks. The developed ANN are for two systems with a bottom water aquifer: vertical well in a radial system, and a horizontal well in a rectangular system. A total of 6 input parameters are needed for the ANN to predict the water saturation distribution for 10 years. The predicted values for the vertical well represent the water saturation distribution around the wellbore at the end of each year for the 10 years. For the horizontal well, the predictions are for the vertical plane that contains the horizontal well.
The examples in this study showed that the accuracy of the prediction is good and matching the numerical simulation results. The high error occurs in the transition zones, because at these zones, the water saturation is changing at a faster rate compared to the water saturation change at zones where the water saturation change is small.

The developed ANN can be used to optimize production, by running the ANN for different scenarios to find the optimum production rate that delay water production and increase oil production. Also, it can be used to select the optimum perforation interval that will increase production of water-free oil and delay water production or reduce it.

This study proposed a solution for water encroachment problems caused by two different boundary conditions. The first part proposed a procedure to estimate the distance to the edge water encroachment front for an oil reservoir. In the second part, an artificial expert system is predicted to understand the water saturation distribution for an oil reservoir with a strong bottom water aquifer. Although, these two proposed solutions are aimed for two different problems, they could be combined to predict water saturation distribution in an oil reservoir that is simultaneously exposed to bottom water drive, and edge water encroachment due to peripheral injection (Fig 5.1).

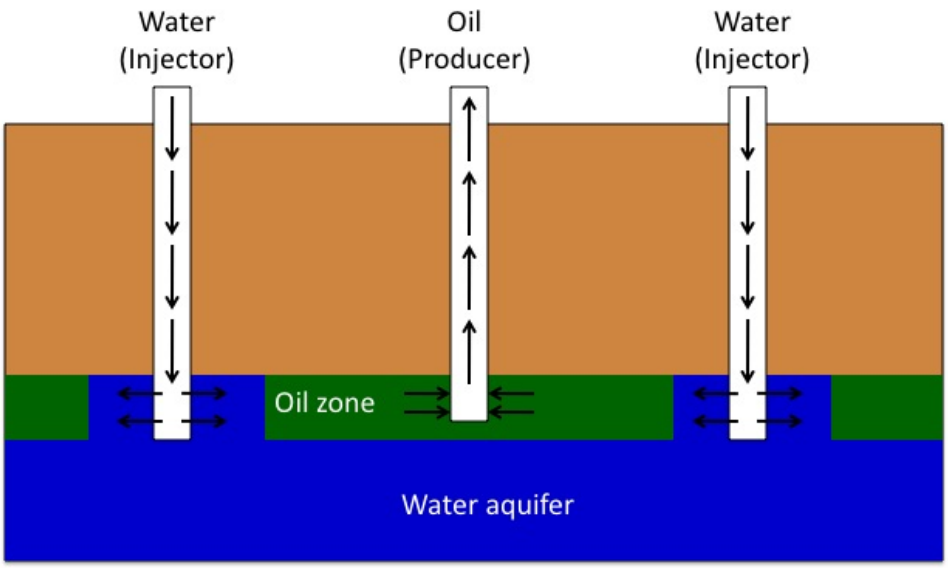

Figure 5.1: Schematic representation of an oil reservoir exposed to bottom water aquifer and edge water encroachment.

Appendix A

Properties used in designing the simulation models for different scenarios for vertical and horizontal wells

Table A.1: Properties used in designing the simulation models for different scenarios for vertical wells

No.	ρ_o, lb/ft^3	q_L, STB/D	μ_o, cp	k_v, md	h_p, ft	h, ft
1	53.76	1,212	3.81	74	24.49	87.46
2	55.07	7,019	9.64	20	117.4	163.1
3	53.02	9,065	6.88	141	86.37	239.9
4	50.82	2,087	2.32	296	26.09	72.48
5	54.21	9,794	1.39	374	43.83	156.5
6	55.28	4,390	8.69	35	38.46	73.96
7	54.48	3,222	9.60	54	22.11	42.53
8	51.44	7,691	6.00	192	15.58	194.7
9	48.06	4,782	5.60	22	50.82	158.8
10	53.35	6,259	7.83	200	30.98	59.59
11	49.92	1,691	2.12	170	56.90	109.4

continue on next page

Table A.1: (Continued)

No.	ρ_o, lb/ft^3	q_L, STB/D	μ_o, cp	k_v, md	h_p, ft	h, ft
12	49.24	4,894	3.73	234	74.84	233.8
13	55.73	9,821	8.96	279	54.26	71.39
14	51.92	10,000	5.62	352	22.12	39.50
15	51.54	7,133	2.51	97	49.12	64.63
16	49.85	6,603	2.76	450	139.6	218.2
17	51.34	7,423	4.50	245	22.42	186.9
18	49.43	4,214	2.21	451	167.5	246.4
19	56.57	8,551	9.42	223	165.6	207.0
20	55.47	552	9.60	498	99.75	226.7
21	56.31	4,330	3.20	229	99.11	145.7
22	57.97	6,456	3.83	92	170.2	193.5
23	53.99	1,935	9.86	129	131.3	172.8
24	48.45	2,640	3.31	63	205.1	223.0
25	49.53	5,573	8.60	120	23.13	144.5
26	54.18	8,259	6.94	128	128.2	213.6
27	57.16	9,002	1.28	31	121.2	202.0
28	50.04	8,291	2.52	401	125.1	208.5
29	48.52	1,325	6.59	246	154.4	241.3
30	50.46	9,374	2.90	398	13.36	55.69
31	50.70	6,989	6.55	397	20.84	27.43
32	57.65	8,521	5.33	186	15.33	191.6
33	52.86	2,565	4.84	350	37.36	155.6
34	48.76	2,563	2.72	404	11.47	71.69
35	52.15	9,032	2.19	207	80.93	224.8
36	51.03	3,910	7.51	358	15.67	195.9
37	55.37	2,689	7.26	409	85.09	163.6
38	55.67	5,660	5.62	193	3.005	37.57
39	53.37	3,278	3.39	394	16.55	25.87

continue on next page

Table A.1: (Continued)

No.	ρ_o, lb/ft^3	q_L, STB/D	μ_o, cp	k_v, md	h_p, ft	h, ft
40	53.10	3,187	2.34	244	43.24	120.1
41	53.31	4,384	1.32	455	40.19	200.9
42	51.84	2,013	9.71	354	153.6	202.1
43	56.49	4,001	2.59	373	77.03	106.9
44	50.01	8,405	7.12	243	44.50	48.37
45	52.09	9,571	9.57	482	111.5	174.3
46	50.54	9,556	8.21	487	12.62	45.10
47	53.40	3,902	8.00	427	26.78	223.1
48	55.72	5,266	4.26	490	120.0	187.5
49	50.63	7,592	5.59	467	77.54	193.8
50	51.03	4,082	2.75	114	220.9	230.1
51	57.16	5,963	4.40	259	19.56	40.76
52	51.34	8,598	2.95	280	93.28	179.3
53	56.89	3,915	8.72	307	47.78	199.1
54	52.62	3,866	1.70	365	79.22	198.0
55	50.15	5,510	3.24	55	142.8	238.0
56	51.71	7,868	4.38	229	55.77	82.01
57	53.23	2,198	4.95	119	28.53	39.63
58	53.68	5,335	9.12	420	5.356	26.78
59	49.79	6,945	6.93	301	117.8	173.3
60	56.05	3,960	3.18	299	10.58	66.15
61	49.40	4,983	5.03	256	141.6	221.3
62	56.37	8,945	1.84	339	10.95	30.42
63	52.95	2,832	4.38	68	115.4	160.4
64	48.65	7,659	8.91	200	20.52	171.0
65	51.49	9,660	5.49	324	90.48	205.6
66	57.80	1,577	4.95	389	37.00	71.16
67	53.02	4,129	3.33	370	24.56	55.82

continue on next page

Table A.1: (Continued)

No.	ρ_o, lb/ft^3	q_L, STB/D	μ_o, cp	k_v, md	h_p, ft	h, ft
68	53.31	752	2.57	345	9.541	79.51
69	57.20	2,401	6.62	260	17.70	27.66
70	52.21	5,129	6.36	10	38.24	159.3
71	52.87	7,097	7.50	365	24.48	47.09
72	52.29	8,012	5.62	254	57.54	110.6
73	54.35	6,689	4.20	83	59.51	92.98
74	50.46	8,031	6.59	231	17.70	221.3
75	51.79	5,378	8.76	221	88.25	200.5
76	55.92	5,982	3.59	367	60.72	138.0
77	50.85	3,240	3.09	56	49.54	112.6
78	51.79	1,307	3.42	273	97.43	221.4
79	52.54	7,189	1.96	175	121.8	145.0
80	48.37	9,551	8.36	248	29.28	40.67
81	49.22	5,185	8.48	399	65.13	108.5
82	53.69	3,054	4.06	425	61.13	152.8
83	51.99	9,174	4.22	405	18.93	157.8
84	52.36	9,116	8.18	63	44.90	102.0
85	50.91	8,849	5.89	189	36.86	230.4
86	56	3,950	8.5	290	37.5	187.5
87	57	3,900	9	310	58.8	210
88	52	3,816	1.6	360	69.3	192.5
89	53	3,916	1.8	370	88	200
90	52.4	3,846	1.65	363	78.7	196.7
91	52.8	3,886	1.75	367	79.7	199.2
92	52.5	3,856	1.69	364	79	197.5
93	52.7	3,876	1.71	366	79.4	198.5
94	50	5,500	3.1	40	126	225
95	51	5,550	3.3	60	160	250

continue on next page

Table A.1: (Continued)

No.	ρ_o, lb/ft^3	q_L, STB/D	μ_o, cp	k_v, md	h_p, ft	h, ft
96	50.05	5,508	3.1	54	141	235
97	50.25	5,512	3.3	56	144	240
98	51.6	7,866	4.28	227	52.7	77.5
99	51.8	7,870	4.48	231	56.1	82.5
100	53.13	2,196	4.86	118	26.82	37.25
101	53.33	2,200	5.06	120	30.42	42.25
102	53	5,300	9	400	4	25
103	54	5,400	9.3	440	6.6	27.5
104	49	6,900	6.8	290	104	162.5
105	50	7,000	7.1	310	135	187.5
106	56.14	2,041	6.79	35	68.64	156.0
107	57.05	8,046	4.40	343	17.59	146.6
108	49.26	3,457	8.30	26	132.4	220.7
109	57.13	5,521	5.79	40	40.59	84.57
110	54.32	2,074	4.15	263	65.66	96.56
111	48.97	6,219	9.45	53	35.23	51.82
112	50.78	2,998	8.88	410	151.3	236.4
113	53.46	6,714	5.95	410	13.61	170.2
114	57.57	7,048	6.60	363	15.94	132.8
115	57.64	7,607	6.28	79	54.03	168.8
116	49.57	4,780	2.86	332	76.73	147.5
117	57.70	1,296	3.71	262	109.2	170.6
118	57.57	2,675	5.23	487	58.94	147.3
119	52.85	9,177	3.07	326	149.7	187.2
120	56.00	1,948	8.59	401	102.6	142.5
121	49.41	8,345	2.75	230	228.6	248.5
122	52.21	5,614	3.03	219	38.58	74.20
123	57.15	9,963	2.53	414	15.61	48.80

continue on next page

Table A.1: (Continued)

No.	ρ_o, lb/ft^3	q_L, STB/D	μ_o, cp	k_v, md	h_p, ft	h, ft
124	55.92	1,243	3.04	46	5.961	49.68
125	57.59	4,705	4.92	71	23.58	39.30
126	54.55	1,513	3.79	91	88.18	116.0
127	48.35	9,638	9.31	199	55.38	125.8
128	56.49	544	4.87	417	12.87	107.3
129	57.33	7,862	2.66	403	55.10	196.7
130	54.78	8,264	9.14	35	33.25	166.2
131	55.57	8,753	9.81	203	55.63	198.6
132	55.43	1,302	4.94	266	103.3	234.8
133	51.92	4,298	2.00	211	126.8	243.8
134	54.55	2,969	3.32	330	32.73	68.20
135	49.71	8,101	4.67	316	47.24	56.24
136	55.06	4,598	6.35	150	94.46	181.6
137	48.31	9,151	3.35	219	42.42	46.10
138	50.76	2,228	6.42	13	91.65	143.2
139	48.46	3,006	7.40	492	132.7	144.3
140	48.97	1,883	2.99	88	61.25	218.7
141	56.23	1,793	2.05	58	91.18	134.0
142	54.94	8,758	3.67	189	36.32	113.5
143	51.17	6,007	3.86	103	112.6	176.0
144	57.50	5,724	4.81	247	130.4	191.7
145	48.34	1,877	5.57	173	17.04	142.0
146	52.38	8,604	1.76	476	28.90	103.2
147	51.81	6,410	3.36	461	14.09	58.74
148	55.65	3,834	8.20	31	100.3	156.8
149	55.95	5,376	1.26	370	67.18	83.98
150	49.86	4,317	9.35	138	12.60	35.00
151	52.89	1,222	7.57	214	148.0	194.8

continue on next page

Table A.1: (Continued)

No.	ρ_o, lb/ft^3	q_L, STB/D	μ_o, cp	k_v, md	h_p, ft	h, ft
152	52.45	2,779	5.39	276	54.14	79.62
153	54.46	1,672	6.20	472	4.981	124.5
154	55.09	2,247	3.13	212	107.8	179.7
155	55.54	2,780	5.12	492	42.33	105.8
156	50.76	4,464	9.66	154	167.7	190.6
157	54.79	972	5.92	352	4.552	113.8
158	54.55	9,076	5.69	335	85.80	178.7
159	49.62	9,475	3.08	272	80.70	183.4
160	49.18	5,163	5.40	351	59.76	124.5
161	52.98	5,148	6.61	335	22.34	29.40
162	57.59	3,708	7.11	93	31.82	99.44
163	51.40	9,051	4.55	68	91.55	120.4
164	53.85	4,008	4.30	500	41.18	85.81
165	50.23	1,556	9.89	90	5.546	69.33
166	55.51	7,912	1.33	21	41.97	209.8
167	50.55	4,203	8.96	283	87.64	121.7
168	53.05	2,796	9.21	442	107.8	224.7
169	54.99	4,337	8.16	336	22.60	113.0
170	56.90	1,416	1.88	99	71.29	198.0
171	57.59	1,754	3.35	188	68.56	114.2
172	53.47	9,449	4.01	233	41.38	206.9
173	49.38	9,583	7.11	491	140.3	194.8
174	49.49	5,964	2.22	82	30.77	109.9
175	50.57	1,068	7.49	428	64.77	73.60
176	56.40	2,730	1.96	324	56.79	202.8
177	50.54	3,855	6.88	191	181.3	238.5
178	56.14	8,301	5.44	100	19.74	98.70
179	50.43	646	8.01	217	56.33	176.0

continue on next page

Table A.1: (Continued)

No.	ρ_o, lb/ft^3	q_L, STB/D	μ_o, cp	k_v, md	h_p, ft	h, ft
180	57.29	909	7.43	244	14.84	123.6
181	51.49	2,105	9.13	65	119.0	212.5
182	49.96	6,667	9.01	297	134.6	197.9
183	50.51	7,451	4.00	117	35.07	62.63
184	54.16	6,654	7.28	195	96.33	218.9
185	52.73	4,784	2.78	294	158.5	247.7
186	51.51	5,697	1.27	130	90.07	140.7
187	56.30	3,315	7.69	149	152.2	223.9
188	53.85	7,575	5.50	310	100.6	157.3
189	53.49	2,295	5.31	136	55.03	59.81
190	57.17	7,024	9.14	413	16.79	69.96
191	50.85	2,243	6.48	491	79.26	116.5
192	55.57	4,001	6.55	366	46.43	193.4
193	55.53	6,443	8.73	175	33.72	210.7
194	51.80	7,912	8.24	294	121.6	202.7
195	53.67	1,271	6.19	58	42.53	96.66
196	48.75	9,329	2.64	454	69.67	145.1
197	48.53	7,869	3.15	440	28.95	45.23
198	53.30	5,125	8.97	410	38.10	50.13
199	55.79	4,641	1.25	134	20.03	55.66
200	57.34	4,744	5.40	299	113.7	177.6
201	49.29	3,410	2.51	16	60.02	136.4
202	53.68	5,331	9.80	216	54.14	67.68
203	52.69	5,352	7.41	160	109.1	136.3
204	48.11	8,267	5.50	85	16.29	58.21
205	51.37	8,051	5.23	93	22.42	37.36
206	49.9	6,990	7	309	133.2	185
207	50.1	7,010	7.2	311	136.8	190

continue on next page

Table A.1: (Continued)

No.	ρ_o, lb/ft^3	q_L, STB/D	μ_o, cp	k_v, md	h_p, ft	h, ft
208	49.95	6,995	7.05	309	134.1	186.2
209	50.05	7,005	7.15	311	135.9	188.7
210	48.95	6,890	6.75	289	102.4	160
211	48.9	6,895	6.7	291	103.2	161.2
212	49.05	6,905	6.85	289	105.6	165
213	49.1	6,910	6.9	291	104.8	163.7
214	53.23	2,190	4.96	119	28.62	39.75
215	53.3	2,195	5.01	121	29.52	41
216	53.43	2,210	5.16	119	32.22	44.75
217	53.36	2,205	5.11	121	31.32	43.5
218	53.03	2,186	4.76	117	25.02	34.75
219	53.08	2,191	4.81	119	25.92	36
220	53.23	2,206	4.96	117	28.62	39.75
221	53.18	2,201	4.91	119	27.72	38.5
222	51.5	7,856	4.18	226	51	75
223	51.55	7,861	4.23	228	51.85	76.25
224	51.7	7,876	4.38	226	54.4	80
225	51.65	7,871	4.33	228	53.55	78.75
226	50.15	5,502	3.2	55	142.5	237.5
227	50.2	5,507	3.25	57	143.2	238.7
228	50.35	5,522	3.4	55	145.5	242.5
229	50.3	5,517	3.35	57	144.7	241.2
230	52.9	5,290	8.9	399	3.6	22.5
231	52.95	5,295	8.95	401	3.8	23.75
232	53.1	5,310	9.1	399	4.4	27.5
233	53.05	5,305	9.05	401	4.2	26.25

Table A.2: Properties used in designing the simulation models for different scenarios for horizontal wells

No.	ρ_o, lb/ft^3	q_L, STB/D	μ_o, cp	k_v, md	h, ft	h_L, ft	h_d, ft
1	52.92	2,672	7.72	16	111.38	1,000	40.84
2	52.28	4,962	2.35	229	156.71	3,400	15.67
3	50.78	4,685	3.62	75	143.37	3,400	43.01
4	49.47	6,963	9.25	8	99.74	2,200	29.92
5	54.22	6,195	5.84	382	206.22	1,800	34.37
6	54.48	3,353	1.01	390	164.35	1,800	38.35
7	57.09	6,172	5.88	404	79.37	1,400	13.23
8	51.76	6,286	9.90	253	136.47	3,400	40.94
9	51.67	8,357	5.86	464	131.24	1,000	39.37
10	50.89	5,319	2.05	192	210.79	2,600	105.4
11	54.15	3,606	1.50	209	219	1,800	7.3
12	54.17	5,989	8.33	291	191.47	3,000	19.15
13	52.91	6,637	6.81	384	38.33	1,000	3.83
14	50.32	5,418	5.91	115	208.04	1,400	48.54
15	56.39	2,776	7.59	233	119.66	3,000	27.92
16	50.06	6,704	4.83	278	200.93	1,000	33.49
17	57.08	4,787	8.71	296	155.35	2,600	46.61
18	54.00	1,329	1.91	360	138.41	2,200	59.98
19	57.45	5,238	2.29	425	25.98	2,200	7.79
20	51.43	1,692	1.36	176	61.57	1,400	2.05
21	56.43	7,423	3.53	38	69.51	2,200	25.49
22	54.31	6,869	9.14	279	34.07	3,000	1.14
23	50.58	8,313	5.28	200	56.36	2,600	13.15
24	51.85	6,814	6.83	286	134.74	1,800	4.49
25	50.53	7,580	2.18	152	37.37	1,000	16.19
26	55.09	2,826	4.24	189	218.75	600	36.46
27	53.99	2,465	3.70	219	41.73	3,400	9.74
28	52.27	2,246	5.78	232	121.03	1,000	12.1

continue on next page

Table A.2: (Continued)

No.	ρ_o, lb/ft^3	q_L, STB/D	μ_o, cp	k_v, md	h, ft	h_L, ft	h_d, ft
29	49.99	3,596	3.51	349	179.45	1,800	89.73
30	56.72	9,958	5.41	27	22.79	2,200	6.84
31	56.81	5,462	4.42	8	57.81	2,600	9.63
32	49.29	7,447	2.43	110	99.31	2,200	16.55
33	56.83	6,688	7.52	133	32.3	3,000	5.38
34	51.22	4,356	6.56	87	205.46	2,200	75.34
35	56.88	1,511	8.06	234	66.61	1,800	15.54
36	49.52	2,871	9.28	19	65.78	3,000	6.58
37	48.76	6,962	7.86	454	131.71	600	48.29
38	56.36	8,193	3.46	25	75.02	1,000	27.51
39	51.96	3,682	2.74	384	99.71	600	9.97
40	49.27	5,510	8.35	320	110.32	2,200	40.45
41	49.55	8,853	6.85	71	23.29	1,000	11.64
42	51.28	1,609	1.68	385	52.84	3,400	22.9
43	55.26	7,767	1.76	333	98.03	3,000	9.8
44	48.33	9,970	9.08	144	34.23	3,000	3.42
45	52.29	6,561	8.06	155	74.77	1,400	7.48
46	56.94	2,782	8.27	396	48.79	1,400	14.64
47	54.96	1,350	3.69	436	133.83	1,000	31.23
48	50.49	6,766	2.65	117	87.6	1,400	2.92
49	53.42	9,940	7.65	445	151.3	600	75.65
50	50.31	2,727	4.45	468	152.61	1,800	55.96
51	54.41	4,100	2.71	86	235.29	1,800	39.21
52	52.63	9,993	9.02	383	194.11	1,000	19.41
53	53.26	5,353	2.58	479	230.63	3,400	99.94
54	56.80	2,003	9.48	212	149.75	2,200	34.94
55	55.65	9,294	7.84	332	101.45	1,400	30.43
56	54.31	1,580	4.06	173	172.7	2,600	28.78

continue on next page

Table A.2: (Continued)

No.	ρ_o, lb/ft^3	q_L, STB/D	μ_o, cp	k_v, md	h, ft	h_L, ft	h_d, ft
57	50.80	7,096	8.44	232	130.74	3,400	65.37
58	48.36	3,808	6.24	130	50.6	2,200	5.06
59	53.97	1,438	9.49	418	184.89	3,000	67.79
60	56.88	2,698	7.25	314	178.97	1,800	5.97
61	48.85	6,584	3.74	97	110.41	600	11.04
62	56.45	9,738	4.49	337	95.22	1,400	15.87
63	54.71	1,743	6.81	224	118.23	600	43.35
64	51.38	8,498	2.70	344	146.47	3,400	34.18
65	55.73	2,215	8.76	59	37.49	1,000	6.25
66	55.53	7,587	6.01	137	25.29	3,000	9.27
67	52.06	4,896	2.41	331	127.33	1,800	21.22
68	55.97	5,549	6.88	72	23.29	3,000	10.09
69	50.59	5,573	8.01	395	85.5	1,400	8.55
70	49.57	4,780	4.00	401	223.57	2,200	81.98
71	56.99	8,201	1.27	464	207.34	2,200	34.56
72	52.99	1,410	9.83	87	20.41	1,400	2.04
73	52.80	3,300	1.69	226	33.1	2,200	3.31
74	51.54	7,201	6.48	352	54.83	3,000	5.48
75	48.26	8,480	4.01	321	200.79	1,400	20.08
76	54.50	6,684	6.08	254	58.07	1,000	9.68
77	57.75	9,930	1.46	29	138.33	1,800	23.05
78	49.57	8,274	6.09	38	148	3,000	24.67
79	49.74	3,068	7.42	198	180.02	1,000	54.01
80	57.24	6,440	3.31	276	52.27	2,200	5.23
81	57.94	9,793	2.63	339	159.87	1,400	15.99
82	48.26	5,770	4.45	134	36.01	1,400	15.6
83	55.11	6,521	9.69	404	43.85	1,800	19
84	57.09	6,071	5.07	453	56.79	3,400	5.68

continue on next page

Table A.2: (Continued)

No.	ρ_o, lb/ft^3	q_L, STB/D	μ_o, cp	k_v, md	h, ft	h_L, ft	h_d, ft
85	54.25	9,413	4.39	95	87.81	2,600	32.2
86	48.84	5,208	4.91	127	110.06	1,400	11.01
87	52.35	6,051	5.37	485	139.28	2,600	32.5
88	54.78	7,790	3.66	474	24.32	2,600	10.54
89	54.77	8,216	4.11	454	91.24	3,400	3.04
90	56.94	1,229	2.07	321	85.26	600	19.9
91	51.80	9,421	3.42	401	119.89	1,000	11.99
92	54.51	4,572	2.04	305	132.62	2,200	4.42
93	57.15	8,817	6.43	105	229.9	2,600	68.97
94	55.83	6,179	6.13	359	93.7	1,800	28.11
95	52.26	4,672	4.05	201	74.05	3,000	7.41
96	50.30	4,177	3.00	331	129.84	2,200	38.95
97	57.42	3,505	5.53	124	68.53	1,400	29.7
98	55.79	6,461	6.26	170	150.45	3,000	45.13
99	50.55	9,719	5.64	228	16.25	2,200	2.71
100	56.69	9,014	8.23	322	199.53	3,000	86.46
101	53.39	4,300	6.05	45	175.09	3,000	75.87
102	57.43	5,586	6.32	377	100.02	3,000	16.67
103	55.15	8,518	7.66	374	110.9	2,200	33.27
104	55.98	8,913	8.91	262	118.34	1,800	27.61
105	53.22	9,356	6.64	196	86.99	1,400	26.1
106	54.04	9,290	1.52	292	146.17	3,400	63.34
107	52.63	8,097	1.15	379	180.03	2,600	66.01
108	51.83	9,559	2.22	147	90.96	1,400	21.22
109	48.35	1,583	4.28	208	22.6	1,400	6.78
110	48.92	8,496	9.95	466	147.83	2,600	73.91
111	50.02	2,481	1.35	151	199.83	3,400	86.59
112	48.36	5,470	2.52	293	225.04	3,400	82.51

continue on next page

Table A.2: (Continued)

No.	ρ_o, lb/ft^3	q_L, STB/D	μ_o, cp	k_v, md	h, ft	h_L, ft	h_d, ft
113	56.86	4,796	7.15	430	54.93	2,600	20.14
114	48.23	5,596	6.09	109	160.54	600	80.27
115	55.56	9,041	9.23	393	133.77	1,400	40.13
116	48.52	2,297	1.03	221	47.9	1,400	11.18
117	53.67	8,229	3.48	32	43.19	1,800	15.84
118	51.22	5,179	6.67	429	185.06	3,000	43.18
119	57.31	1,050	2.23	115	206.5	1,800	48.18
120	48.03	1,754	9.73	453	91.57	1,400	21.37
121	52.26	1,478	9.35	86	15.45	2,200	6.7
122	55.80	4,487	8.47	435	102.32	1,000	10.23
123	50.35	1,090	6.74	81	32.8	2,600	14.21
124	52.43	5,159	3.40	367	143.49	1,000	33.48
125	55.04	8,675	5.23	374	40.92	2,200	12.28
126	57.37	8,373	2.81	282	27.41	3,000	2.74
127	51.98	1,168	8.14	145	56.57	600	9.43
128	48.79	5,838	3.57	258	182.3	1,000	30.38
129	56.29	9,002	4.36	166	54.3	2,200	12.67
130	51.35	5,579	4.10	264	164.96	3,400	38.49
131	52.47	2,747	7.02	276	55.25	1,400	12.89
132	53.54	5,462	8.46	58	28.41	1,400	2.84
133	49.04	2,673	7.81	492	198.38	2,200	33.06
134	53.32	2,353	5.92	182	32.98	2,200	12.09
135	49.94	7,647	7.89	256	17.51	1,400	4.09
136	56.25	8,920	8.12	494	136.63	2,200	31.88
137	54.84	1,045	1.34	169	228.8	3,000	83.89
138	49.49	8,238	6.01	113	62.95	3,400	23.08
139	48.09	4,523	4.64	482	223.58	1,800	52.17
140	54.79	2,792	4.13	241	54.65	1,400	9.11

continue on next page

Table A.2: (Continued)

No.	ρ_o, lb/ft^3	q_L, STB/D	μ_o, cp	k_v, md	h, ft	h_L, ft	h_d, ft
141	48.66	3,625	7.92	192	211.28	1,000	77.47
142	55.62	5,583	2.98	165	107.41	1,800	53.7
143	52.32	3,361	2.40	54	106.73	2,200	24.9
144	48.32	4,752	5.28	361	21.54	3,400	7.9
145	53.67	2,313	2.88	148	133.24	2,200	22.21
146	54.31	5,703	3.45	290	127.72	2,600	38.32
147	48.93	2,110	5.29	71	66.95	600	11.16
148	55.29	5,559	5.40	210	58.75	1,800	13.71
149	50.44	7,168	1.81	272	143.88	1,000	23.98
150	53.06	7,462	4.23	156	64.18	2,600	23.53
151	53.11	5,337	5.43	395	59.96	2,600	6
152	48.66	4,780	3.23	300	118.98	3,000	27.76
153	52.99	7,775	6.74	409	33.61	2,200	5.6
154	51.32	9,593	1.54	416	173.85	1,000	40.57
155	48.59	3,099	7.31	335	191.43	3,000	19.14
156	51.62	2,231	5.19	63	82.27	1,400	24.68
157	48.39	1,876	2.15	322	224.28	2,200	22.43
158	50.93	4,755	2.51	222	116.27	2,200	19.38
159	53.98	1,855	5.54	142	199.91	3,000	59.97
160	48.11	7,891	2.19	288	136.74	1,000	41.02
161	57.76	7,453	3.25	445	46.69	1,800	7.78
162	48.27	8,328	5.83	466	154.46	2,200	36.04
163	57.29	3,910	8.65	133	131.42	1,000	56.95
164	57.43	5,460	4.04	367	20.02	3,000	7.34
165	52.62	7,646	4.82	168	104.95	3,000	31.49
166	49.52	3,349	3.22	108	96.32	1,800	28.9
167	51.47	8,706	3.72	157	156.4	3,000	5.21
168	50.95	5,159	1.33	37	235.5	1,400	102.05

continue on next page

Table A.2: (Continued)

No.	ρ_o, lb/ft^3	q_L, STB/D	μ_o, cp	k_v, md	h, ft	h_L, ft	h_d, ft
169	57.27	9,442	6.75	311	220.36	600	80.8
170	51.70	5,990	4.30	332	165.63	3,400	27.6
171	50.80	7,534	7.82	374	104.73	600	10.47
172	53.39	6,339	7.59	447	163.18	1,400	16.32
173	56.99	3,040	3.91	438	28.02	1,400	0.93
174	53.50	9,710	9.55	200	57.27	1,400	5.73
175	57.09	1,376	1.26	184	123.55	2,600	12.36
176	53.62	2,844	9.70	485	70.81	3,400	35.41
177	52.33	8,471	9.33	237	185.43	3,000	80.35
178	56.99	9,715	7.78	243	185.87	600	43.37
179	57.69	8,024	8.35	113	24.1	1,400	4.02
180	55.16	2,953	8.49	310	77.22	1,800	28.31
181	55.83	6,634	3.81	265	88.42	1,800	44.21
182	56.59	1,626	9.34	364	163.99	600	49.2
183	48.90	1,342	2.58	485	15.2	1,400	0.51
184	51.71	3,692	9.92	337	196.94	1,400	19.69
185	51.65	9,577	8.63	187	211.62	600	21.16
186	55.39	1,087	5.95	106	175.85	1,000	52.75
187	56.33	5,800	8.35	213	104.25	3,400	38.22
188	52.11	5,937	6.45	39	133.13	1,400	66.56
189	52.77	1,780	9.85	451	144.54	3,000	72.27
190	56.39	1,762	7.53	193	134.15	2,200	31.3
191	54.23	4,969	1.68	472	70.44	1,400	16.44
192	55.70	9,061	2.92	279	118.51	1,800	19.75
193	55.24	5,924	4.84	344	220.4	3,400	80.81
194	53.31	5,570	3.87	149	142.9	2,600	52.4
195	54.03	2,875	6.43	55	165.23	1,400	38.55
196	54.57	4,500	1.75	84	45.47	600	10.61

continue on next page

Table A.2: (Continued)

No.	ρ_o, lb/ft^3	q_L, STB/D	μ_o, cp	k_v, md	h, ft	h_L, ft	h_d, ft
197	52.16	8,223	7.88	300	223	3,000	66.9
198	50.71	5,994	6.48	179	190.92	2,600	82.73
199	53.58	9,157	9.18	161	183.34	3,000	6.11
200	54.49	9,418	8.18	98	103.75	1,000	31.13
201	52.10	9,216	7.94	487	60.03	1,800	18.01
202	56.01	8,390	8.10	192	18.7	1,800	1.87
203	52.87	8,344	6.59	424	180.36	1,000	54.11
204	57.92	8,798	2.44	361	214.64	3,000	50.08
205	52.12	8,348	9.65	91	71	3,400	30.77
206	54.19	4,162	7.33	140	182.93	3,000	30.49
207	49.57	4,955	2.64	346	84.03	600	36.41
208	50.89	6,166	3.92	396	130.7	1,000	56.64
209	52.52	5,866	5.67	61	224.82	2,200	97.42
210	54.07	4,881	1.88	30	174.69	1,400	29.12
211	56.80	9,528	2.38	137	88.03	2,600	44.01
212	50.14	3,867	8.97	215	45.45	3,400	1.51
213	54.41	2,551	4.05	455	44.47	600	7.41
214	57.30	9,240	8.18	412	58.01	2,200	21.27
215	57.02	7,165	9.49	422	113.94	600	3.8
216	52.00	7,638	5.82	466	122.3	1,400	53
217	50.63	1,515	5.53	177	108.54	2,600	25.33
218	48.87	2,819	9.03	283	222.66	1,400	81.64
219	50.25	4,074	8.00	497	224.21	2,600	37.37
220	50.47	4,406	4.93	380	77.9	2,200	2.6
221	49.13	9,230	2.10	280	62.03	1,800	22.74
222	49.47	9,919	4.81	354	190.21	2,200	57.06
223	48.62	2,548	2.60	401	185.08	3,000	92.54
224	57.74	2,072	3.34	106	138.66	1,000	50.84

continue on next page

Table A.2: (Continued)

No.	ρ_o, lb/ft^3	q_L, STB/D	μ_o, cp	k_v, md	h, ft	h_L, ft	h_d, ft
225	51.90	3,203	6.72	473	104	600	24.27
226	52.95	3,788	2.46	122	94.9	600	3.16
227	49.42	2,939	1.19	64	33.28	600	9.98
228	56.62	1,211	8.15	262	210.85	2,200	77.31
229	50.34	3,988	3.34	162	96.28	2,600	35.3
230	53.62	6,581	1.66	402	122.59	1,400	53.12
231	54.25	3,350	5.51	39	145.54	3,000	24.26
232	51.10	6,960	9.75	134	98.2	600	29.46
233	54.40	1,322	1.67	469	31.72	3,400	13.75
234	56.33	4,254	2.53	15	58.89	600	13.74
235	53.15	1,172	8.13	264	25.08	2,200	10.87
236	53.23	7,413	7.82	82	27.57	2,200	4.6
237	50.70	4,284	6.97	291	64.63	1,000	19.39
238	52.05	4,704	6.26	189	74.87	1,400	32.45
239	48.96	7,942	7.91	9	121.83	1,400	28.43
240	51.58	4,237	3.56	273	86.78	1,000	2.89
241	56.43	5,676	9.10	128	65.44	3,400	19.63
242	54.98	5,503	8.39	290	65.47	2,200	19.64
243	48.63	8,975	7.05	54	180.61	3,000	54.18
244	54.68	5,369	1.07	137	150.54	1,800	75.27
245	54.50	1,197	7.02	477	42.01	600	12.6
246	54.34	3,359	7.54	467	218.14	2,600	79.99
247	49.11	8,182	8.06	8	85.16	2,200	8.52
248	54.84	9,931	5.28	94	70.94	2,600	11.82
249	51.04	6,359	2.64	332	40.14	2,600	12.04
250	52.96	9,113	4.39	265	20.27	1,400	6.08
251	55.44	2,883	4.88	306	54.88	1,400	12.8
252	54.54	8,958	9.12	14	230.62	1,400	84.56

continue on next page

Table A.2: (Continued)

No.	ρ_o, lb/ft^3	q_L, STB/D	μ_o, cp	k_v, md	h, ft	h_L, ft	h_d, ft
253	55.80	7,824	9.03	283	180.96	2,200	42.22
254	53.97	7,584	8.73	443	164.44	2,200	16.44
255	53.78	5,392	6.44	30	105.36	2,200	38.63
256	51.22	4,723	6.08	364	151.26	2,200	75.63
257	56.25	2,151	1.28	200	102.28	2,200	3.41
258	55.34	1,960	3.54	398	107.09	1,800	53.54
259	51.98	3,590	1.97	424	129.78	2,600	47.59
260	57.98	8,689	5.53	44	161.37	3,400	48.41
261	55.81	1,122	8.08	91	143.13	1,400	62.02
262	55.86	5,680	7.31	435	91.63	600	9.16
263	50.53	1,307	9.36	483	89.51	1,000	20.89
264	57.45	9,087	6.98	419	99.24	1,400	29.77
265	55.34	3,314	7.74	301	29.83	2,600	2.98
266	50.80	4,415	5.71	295	163.03	2,200	70.65
267	49.35	6,298	4.80	316	143.68	1,400	43.1
268	52.20	9,171	3.08	131	174.07	1,000	63.83
269	48.87	6,659	4.69	6	183.9	3,000	55.17
270	56.66	3,476	1.45	315	227.82	3,400	98.72
271	49.07	7,016	2.21	269	149.06	1,800	4.97
272	56.76	2,795	6.91	371	182.68	2,200	54.81
273	54.79	7,924	9.58	379	117.84	1,000	43.21
274	53.98	4,150	7.79	484	237.73	1,400	39.62
275	48.47	1,357	7.63	204	168.63	3,400	5.62
276	56.55	1,441	8.00	338	153.07	3,000	76.53
277	48.26	6,687	7.70	164	80.77	3,000	24.23
278	55.17	2,997	8.02	483	164.26	1,400	16.43
279	57.78	9,992	5.92	119	37.69	1,800	3.77
280	50.89	1,560	1.01	257	66.93	2,200	11.16

continue on next page

Table A.2: (Continued)

No.	ρ_o, lb/ft^3	q_L, STB/D	μ_o, cp	k_v, md	h, ft	h_L, ft	h_d, ft
281	52.60	4,723	1.67	271	157.83	3,000	78.91
282	53.15	9,830	9.70	456	190.64	1,000	19.06
283	49.41	5,456	8.85	127	170.67	1,800	62.58
284	48.98	6,242	1.06	56	177.34	3,000	29.56
285	57.64	7,469	7.62	317	80.65	3,000	8.07
286	52.06	6,520	9.88	203	163.54	2,600	5.45
287	49.70	1,401	7.66	77	158.03	1,800	26.34
288	49.06	8,649	2.71	37	195.07	3,000	32.51
289	53.21	3,481	1.23	101	198.03	600	85.81
290	54.22	3,065	8.35	167	52.98	2,200	12.36
291	48.58	2,568	6.27	71	166.65	3,400	72.22
292	53.75	4,285	8.72	359	78.98	3,000	34.23
293	56.84	2,047	7.25	409	116.37	1,000	3.88
294	53.34	3,703	7.29	280	68.83	3,000	16.06
295	50.91	7,982	7.92	207	149.58	1,000	14.96
296	48.04	3,351	3.91	320	49.07	2,600	4.91
297	48.37	7,240	2.17	232	121.63	1,400	44.6
298	50.46	5,864	4.74	42	204.72	3,400	102.36
299	56.94	9,733	9.27	117	175.93	2,600	41.05
300	49.47	9,576	3.68	458	27.58	1,800	11.95
301	52.81	6,627	6.72	383	36.9	1,000	3.69
302	52.86	6,632	6.77	385	37.65	1,000	3.77
303	52.96	6,642	6.87	383	39.15	1,000	3.92
304	53.01	6,647	6.92	385	39.9	1,000	3.99
305	51	5,400	2	190	240	2,600	104
306	53	5,600	2.1	195	240	3,000	120
307	52.9	6,636	6.81	383	38.31	1,000	3.83
308	52.92	6,638	6.82	385	38.33	1,000	3.83

continue on next page

Table A.2: (Continued)

No.	ρ_o, lb/ft^3	q_L, STB/D	μ_o, cp	k_v, md	h, ft	h_L, ft	h_d, ft
309	52.23	4,960	2.31	228	156	3,400	15.6
310	52.33	4,964	2.41	230	157.35	3,400	15.74
311	50.73	4,683	3.58	74	142.65	3,400	42.8
312	50.83	4,687	3.64	76	144	3,400	43.2
313	51.71	6,281	9.85	252	135.75	3,400	40.73
314	51.8	6,290	9.95	254	137.25	3,400	41.18

Appendix B

MATLAB code for training the Neural Network

```
clear
close all
clc
format long
load input
load output
P = input';
T = output';
[m,n] = size(P);
[m1,n1] = size(T);
[P2,ps2] = removeconstantrows(P);
%normalising the data
[Pn,ps] = mapminmax(P2,-1,1); gives all values between -1 and 1
[Tn,ts] = mapminmax(T,-1,1); gives all values between -1 and 1
[mi,ni] = size(Pn);
[mo,no] = size(Tn);
%The following five lines specify the data for training, validation and testing
trainInd = [1:81,106:233];
valInd = [82:96];
testInd = [97:105];
```

```
[Pn_train,Pn_val,Pn_test,trainInd,valInd,testInd] = divideind(Pn,trainInd,valInd,testInd);
[Tn_train,Tn_val,Tn_test] = divideind(Tn,trainInd,valInd,testInd);
val.T = Tn_val;
val.P = Pn_val;
test.T = Tn_test;
test.P = Pn_test;
%Initiating network parameters
HL1 = 43; state number of neurons in first hidden layer
HL2 = 90; state number of neurons in second hidden layer
net = newff(Pn,Tn,[HL1,HL2],{'tansig'},'traincgp','learngdm','msereg');
%setting training parameters for the network
net.trainParam.goal = 0.0001; accuracy within this range
net.trainParam.epochs = 100; number of iteration sets
net.trainParam.show = 1;
net.trainParam.max_fail = 10000;
%starting training the network
[net,tr] = train(net,Pn_train,Tn_train,[],[],test,val);
%-------------------------------------------------
%--------getting data from the trained network ----------------
%-------------------------------------------------
Tn_train_ann = sim(net,Pn_train);
Tn_test_ann = sim(net,Pn_test);
Tn_val_ann = sim(net,Pn_val);
[m_Te,n_Te] = size(Tn_test);
NP_test = 1:n_Te;
-------------------------------------------------

%denormalising the data sets obtained
%output reversal
T_train = mapminmax('reverse',Tn_train,ts);
T_test = mapminmax('reverse',Tn_test,ts);
T_train_ann = mapminmax('reverse',Tn_train_ann,ts);
T_test_ann = mapminmax('reverse',Tn_test_ann,ts);
T_val = mapminmax('reverse',Tn_val,ts);
```

```
T_val_ann = mapminmax('reverse',Tn_val_ann,ts);
%input reversal
P_train = mapminmax('reverse',Pn_train,ps);
P_val = mapminmax('reverse',Pn_val,ps);
P_test = mapminmax('reverse',Pn_test,ps);
```

Appendix C

Water Saturation Maps for Two different reservoirs for Vertical Wells Using ANN

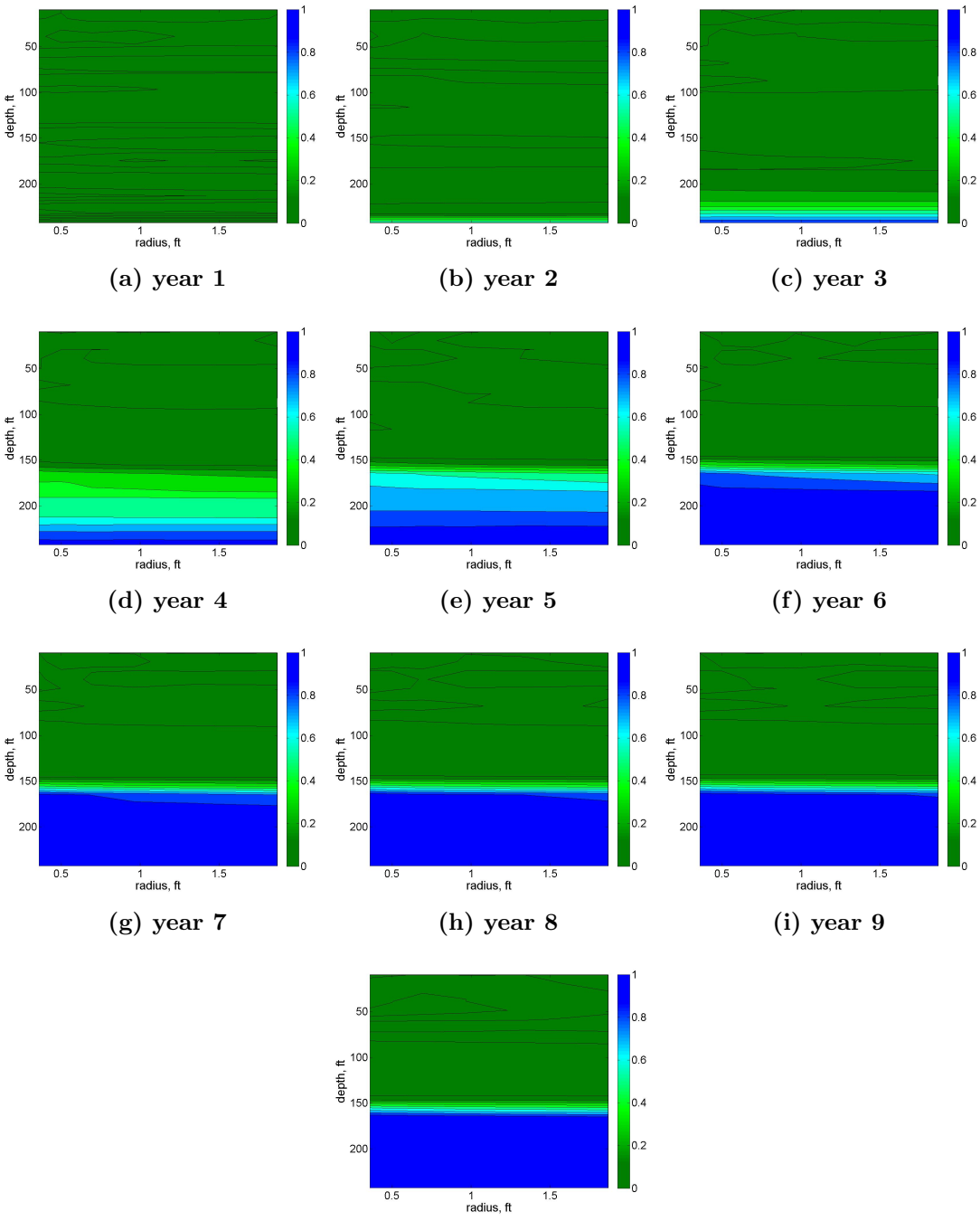

(a) year 1 (b) year 2 (c) year 3

(d) year 4 (e) year 5 (f) year 6

(g) year 7 (h) year 8 (i) year 9

(j) year 10

Figure C.1: Water saturation map for reservoir # 228 using predicted ANN data (Note: vertical permeability for this reservoir is 55 md).

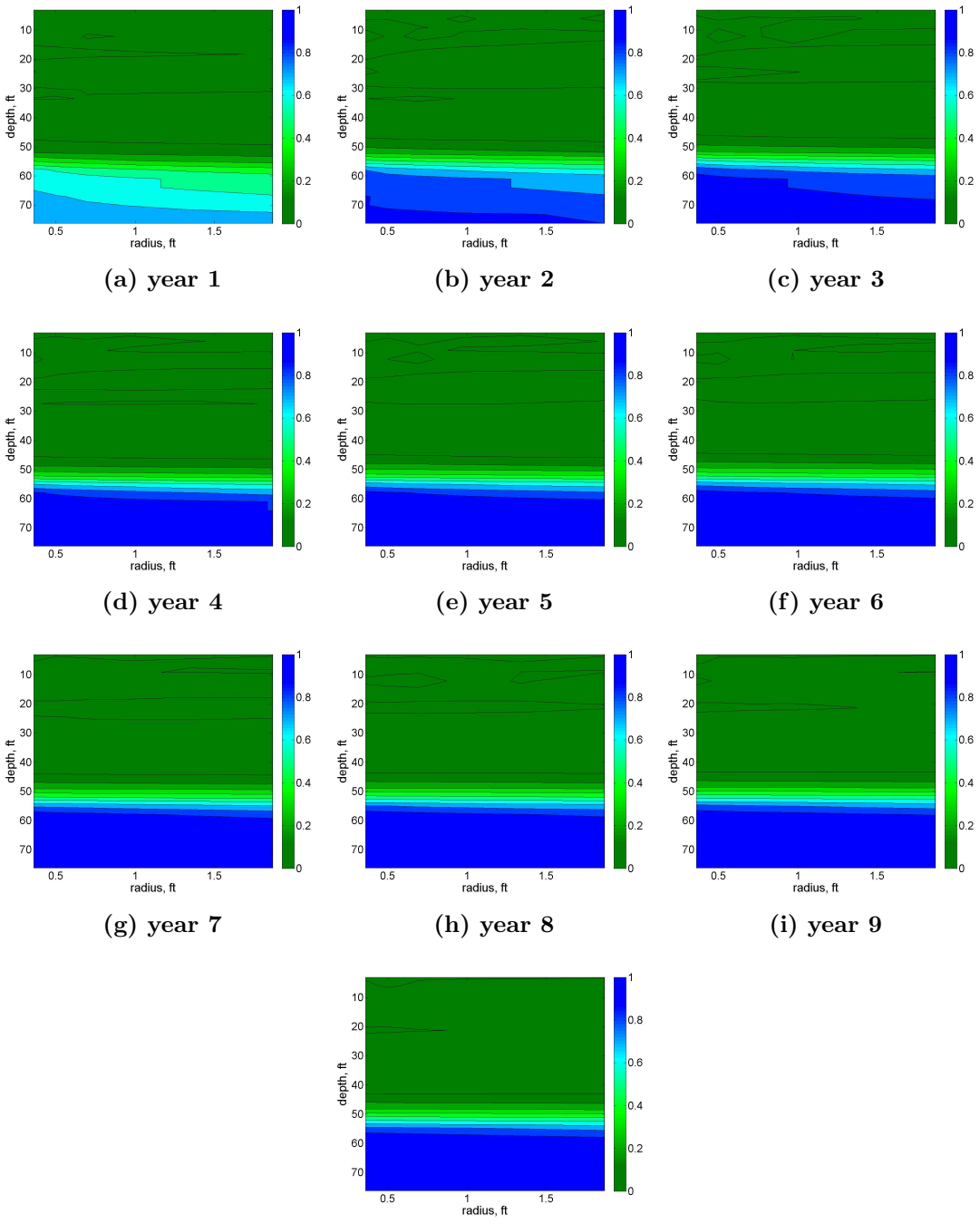

(a) year 1 (b) year 2 (c) year 3

(d) year 4 (e) year 5 (f) year 6

(g) year 7 (h) year 8 (i) year 9

(j) year 10

Figure C.2: Water saturation map for reservoir # 223 using predicted ANN data (Note: vertical permeability for this reservoir is 228 md).

Appendix D

Water Saturation Maps for Two different reservoirs for Horizontal Wells Using ANN

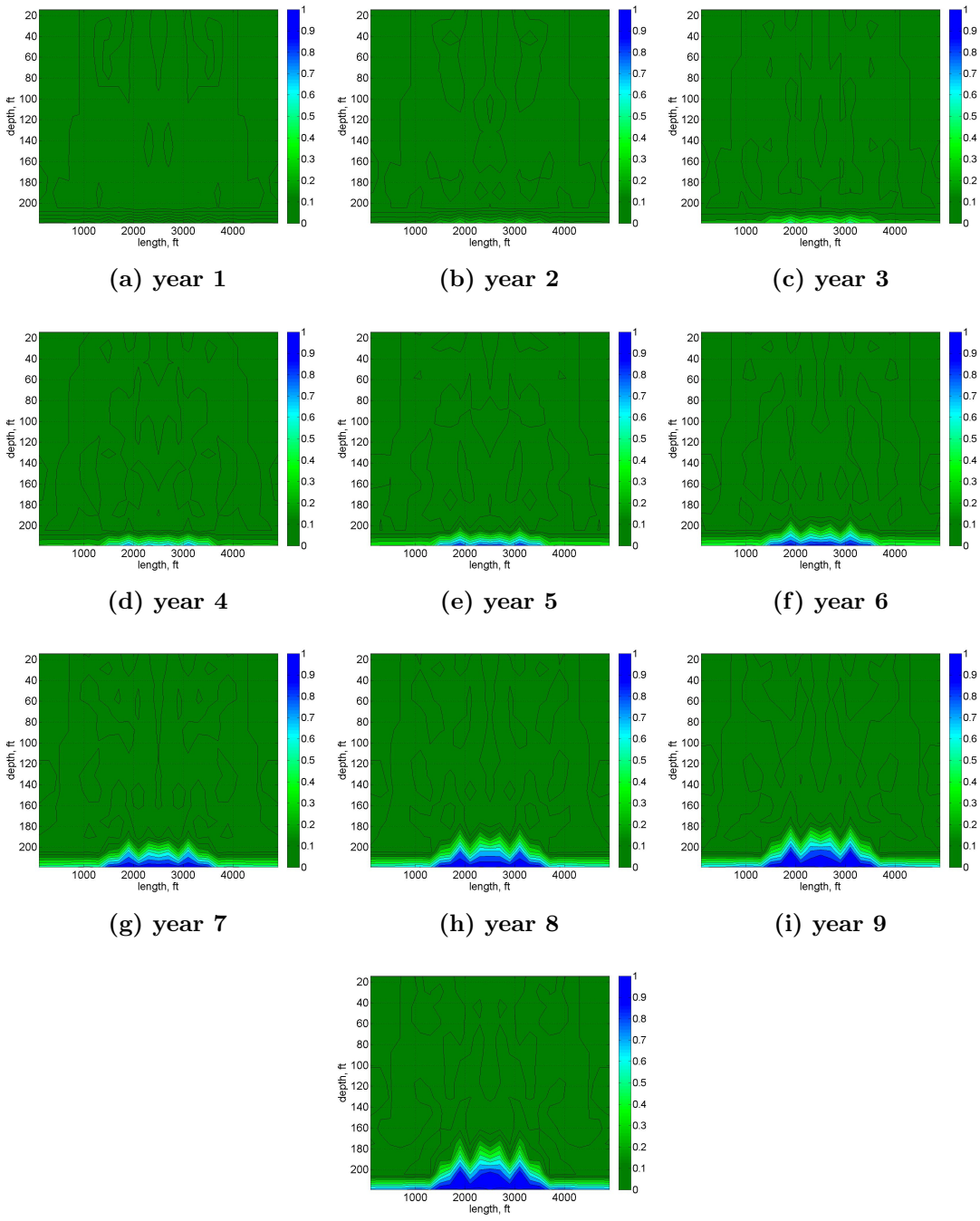

(a) year 1 (b) year 2 (c) year 3

(d) year 4 (e) year 5 (f) year 6

(g) year 7 (h) year 8 (i) year 9

(j) year 10

Figure D.1: Water saturation map for reservoir # 11 using predicted ANN data (Note: vertical permeability for this reservoir is 209 md).

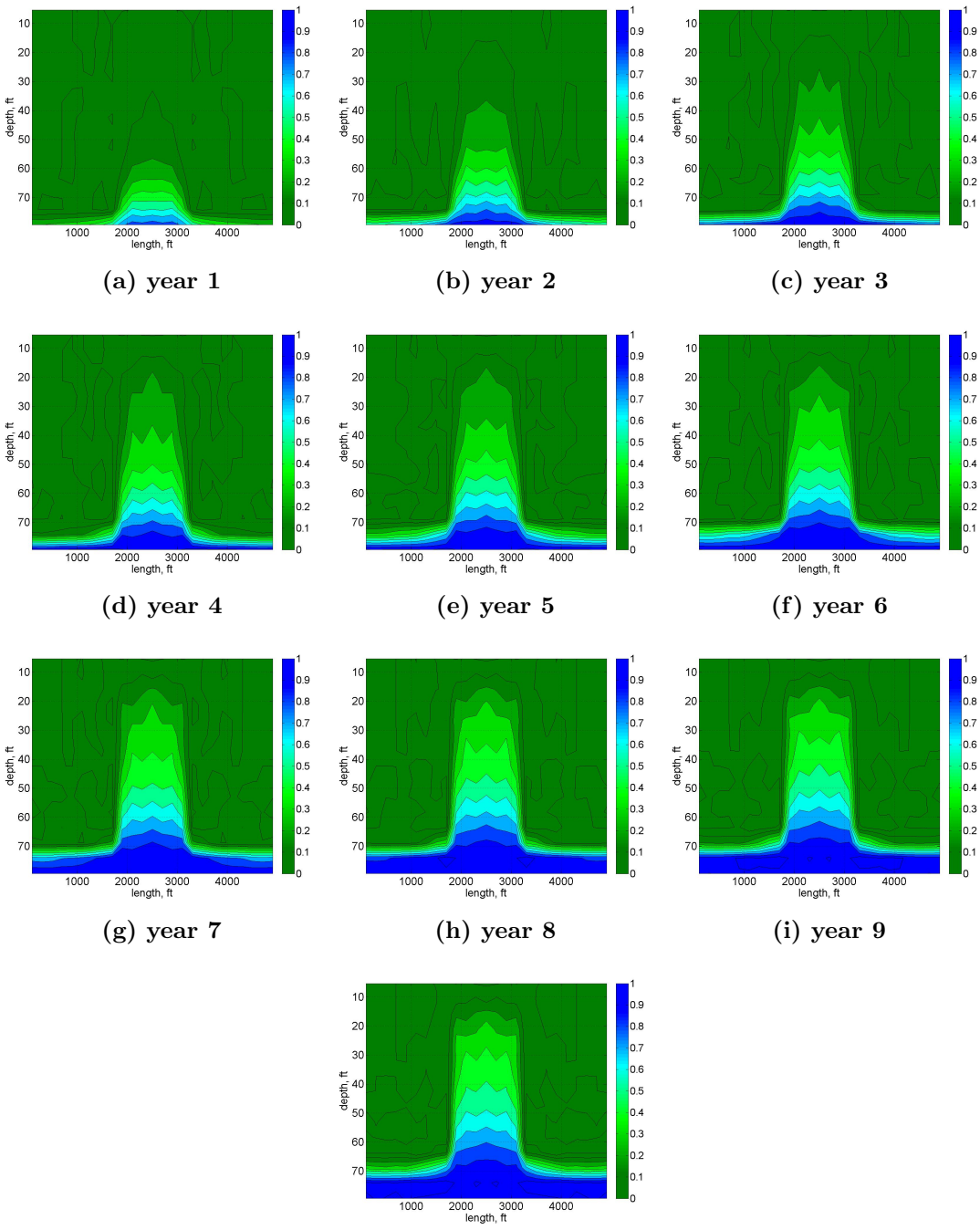

(a) year 1 (b) year 2 (c) year 3

(d) year 4 (e) year 5 (f) year 6

(g) year 7 (h) year 8 (i) year 9

(j) year 10

Figure D.2: Water saturation map for reservoir # 7 using predicted ANN data (Note: vertical permeability for this reservoir is 404 md).

References

Al-Bulushi, N., King, P. R, Blunt, M. J. and Kraaijveld, M.: "Development of Artificial Neural Network Models for Predicting Water Saturation and Fluid Distribution" Journal of Petroleum Science and Engineering, 68 (October 2009) 197-208.

Ali, J. K.: Neural Network: A New Tool for the Petroleum Industry?, paper SPE 27561, 1949.

Ambastha, A. K. and Ramey, H. J., Jr.: Thermal Recovery Well Test Design and Interpretation SPEFE (June 1989) 173-180.

Bixel, H. C. and Poollen, H. K. Van: Pressure Drawdown and Buildup in the Presence of Radial Discontinuities, paper SPE 1516, 1967.

Blades, D. N. and Stright, D. H., Jr.: Predicting High Volume Lift Performance in Wells Coning Water PETSOC-75-04-06-P, 1975.

Bourdet, D., Whittle, T. M., Douglas, A. A. and Pirard, Y. M.: A New Set of Type Curves Simplifies Well Test Analysis, World Oil, 1983.

Bourdet, D., Ayoub, J. A., and Pirard, Y. M.: Use of Pressure Derivative in Well Test Interpretation SPEFE (June 1989) 293; Trans., AIME, 287.

Brown, L. P.: Pressure Transient Behavior of the Composite Reservoir, Paper SPE 14316, 1985.

Byrne, W. B. and Morse, R. A., The Effects of Various Reservoir and Well Parameters on Water Coning Performance paper SPE 4287, 1973.

Carter, R. D.: Pressure Behavior of a Limited Circular Composite Reservoir 1966. SPE 1621-PA.

Hazebroek, P., Rainbow, H., and Mathews, C.S.: Pressure Fall-off in Water injection Wells, paper SPE 925, 1958.

Helle, H.B and Bhatt, A.: "Fluid Saturation from Well Logs using Committee Neural Networks" Petroleum Geoscience, 8 (June 2002) 109-118.

Hurst, W.: Interference between Oil Fields, paper SPE 1335, 1960. Issaka, M. B. and Ambastha, A. K.:A Generalized Pressure Derivative Analysis for Composite Reservoirs, PETSOC 1996-115, 1996.

Kuo, M. C. T. and DesBrisay, C.L.: A Simplified Method for Water Coning Predictions paper SPE 12067, 1983.

Loucks, T. L. and Guerrero, E. T.: Pressure Drop in a Composite Reservoir, Paper SPE 19, 1961.

Mungan, N.: A Theoretical and Experimental Coning Study SPEJ (June 1975) 221-236.

Mortada, M.: Oilfield Interference in Aquifers of Non-Uniform Properties, Paper SPE 1507, 1960.

Muskat, M., and Wyckoff, H. D., An Approximate Theory of Water Coning in Oil Production, Trans AIME, 114, 144-63, 1935.

Odeh, O. S.: Flow Test Analysis for a Well with Radial Discontinuity, Paper SPE 2157, 1969.

Olarewaju, J. S. and Lee, W. J.: A Comprehensive Application of a Composite Reservoir Model to Pressure-Transient Analysis, Paper SPE 16345, 1989.

Rowan, G. and Clegg, M. W.: An Approximate Method for Transient Radial Flow, Paper SPE 156-PA, 1962.

Satman, A. et al.: Interpretation of Injection Well Pressure Transient Data in Thermal Oil Recovery paper SPE 8908, 1980.

Shokir, E.M.El-M.: "Prediction of the Hydrocarbon Saturation in Low Resistivity Formation via Artificial neural Network", Paper SPE 87001, 2004.

Stehfest, H.: Numerical Inversion of Laplace Transform: Algorithm 368 Communication of ACM (Jan. 1970) 47-49.

Tang: Transient Pressure Analysis in Composite Reservoirs, PhD thesis, Stanford University, 1982.

Tiab, D. and Kumar, A.: Detection and Location of Two Parallel Sealing Faults around a Well, Paper SPE 6056, 1980.

Yang, Weiping, Wattenbarger, R. A. Water Coning Calculations for Vertical and Horizontal Wells, paper SPE 22931, 1991.

Vita

Muhammad Alrumah

Education

- Ph. D., Petroleum and Natural Gas Engineering, December 2011, The Pennsylvania State University, University Park, PA, USA.

- M.Sc., Petroleum Engineering, December 2003, Texas A&M University, College Station, TX, USA.

- B. S., Petroleum Engineering, December 1998, Kuwait University, Kuwait.

Work Experience

- Production engineer, Kuwait Oil Company (1999 - 2001), Kuwait.

- Teacher, Petroleum Engineering Department, College of Technological Studies (2004 - 2006), Kuwait.